

Synergistic Antiproliferative Activity of Newly Synthesized Benzimidazole-Based Silver(I) Complexes on MCF-7 and T47D Cell Lines, CT-DNA Interactions Supported by Computational Studies

Naima Munir, Navin Gürbüz, Gul-e-Saba Chaudhry,* İsmail Özdemir,* Muhammad Sarfraz, Betül Şen, Muhittin Aygün, and Muhammad Naveed Zafar*



Cite This: *ACS Omega* 2025, 10, 13278–13295



Read Online

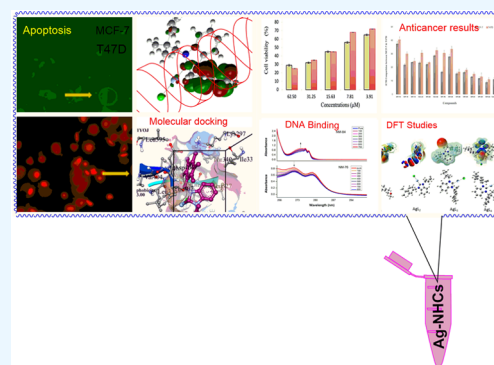
ACCESS |

Metrics & More

Article Recommendations

Supporting Information

ABSTRACT: This article reports the synthesis, characterization, and antitumor properties of newly synthesized benzimidazole-based Ag(I)-(BNHCs) complexes from their proligands. All of the compounds underwent comprehensive characterization using techniques such as ^1H , COSY, ^{13}C NMR, IR spectroscopy, electrospray ionization (ESI)-mass, elemental, and single-crystal X-ray diffraction (XRD) analysis. Density functional theory (DFT) studies were carried out to observe the electronic effects of bound ligands to modulate the selectivity and reactivity of silver complexes. Time-dependent DFT (TD-DFT) studies assessed the optical properties of synthesized complexes and were further highlighted by orbital contributions with oscillator strengths. All compounds were tested against breast cancer MCF-7 and T47D cell lines. The synergistic effects of benzimidazole-incorporated aryl constituent structuring silver complexes were also observed. Nearly all silver complexes have been found to be promising anticancer agents with the added benefit of low cytotoxic effects toward normal cells. Intriguingly, $[\text{AgL}^4(\text{Cl})]$ exhibited the best cytotoxic activity among our screened complexes as IC_{50} values for both MCF-7 and T47D were 9 ± 1.04 and 11 ± 1.41 , respectively. The apoptosis mode of cell death was confirmed by phosphatidylserine exposure and annexin V/PI staining imaging method. CT-DNA interactions of the most active silver complex ($[\text{AgL}^4(\text{Cl})]$) and its proligand ($\text{HL}^4(\text{Cl})$) were carried out to support the mode of compound-DNA interaction. Strong DNA binding affinities (K_b) with compounds through electrostatic and intercalation modes induced structural changes in DNA. Moreover, molecular docking studies were carried out to comprehend the possible interactions of compounds with various receptors such as EGFR (epidermal growth factor receptor), VEGFR2 (vascular endothelial growth factor receptors), FGFR (fibroblast growth factor receptor), and SRC (proto-oncogene tyrosine kinase protein) of tyrosine kinase family serves as crucial receptors in breast cancer.



1. INTRODUCTION

Cancer continues to present a substantial burden on global health, underscoring the pressing need for innovative pharmacological strategies.^{1–3} Breast cancer is the second most common cause of cancer-related deaths, accounting for 11.6%, followed by lung cancer and colorectal cancer.^{1,4} Breast cancer onset emerges from the disruption of intricate cellular communication alleyways within mammary epithelial cells.⁵ A convergence of growth dynamics and chemokines inside the tumor microenvironment facilitates a cascade of complex signals that drive the advancement of cancer. These signals engage with a broad spectrum of receptors, including the prominent EGFR (epidermal growth factor receptor) type I receptor of tyrosine kinase (TK) family and VEGFR2 (Vascular endothelial growth factor receptors), FGFR (fibroblast growth factor receptor), SRC (proto-oncogene tyrosine kinase protein) also known as nonreceptor tyrosine kinase protein, and HGFR (Hepatocyte growth factor receptor) is a part of MET gene. The aberrant receptor

activity is responsible for uncontrolled growth and tumor cell proliferation. To comprehend the full aspect of drug design and the mode of action, there is a dire need to understand the root causes that pose significant long-term disease management. These receptors were chosen for docking analysis due to their active involvement in breast cancer cells.

Chemotherapy is a cornerstone of cancer treatment, primarily utilizing carbon-based compounds to target tumor cells. However, with the discovery of Cisplatin,⁶ inorganic compounds emerged as potential anticancer agents accompanying various transition metals, gold(I) and iridium(III),

Received: December 6, 2024

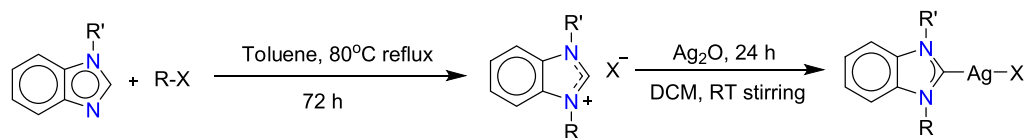
Revised: March 16, 2025

Accepted: March 24, 2025

Published: March 28, 2025



Scheme 1. Synthetic Route to Proligands and Silver-BNHCs Complexes



When R'

Cyclopentyl, X = Br (**1**)

1-(2-methyl-2-phenylpropyl), X = Cl (**2**)

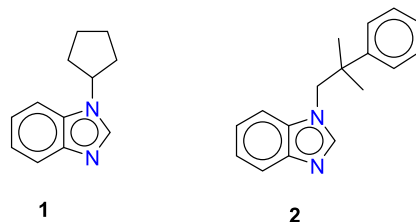
When R,

Methoxyethyl, X = Cl **HL¹(Cl)**

4-tert-Butylbenzyl, X = Br **HL²(Br)**

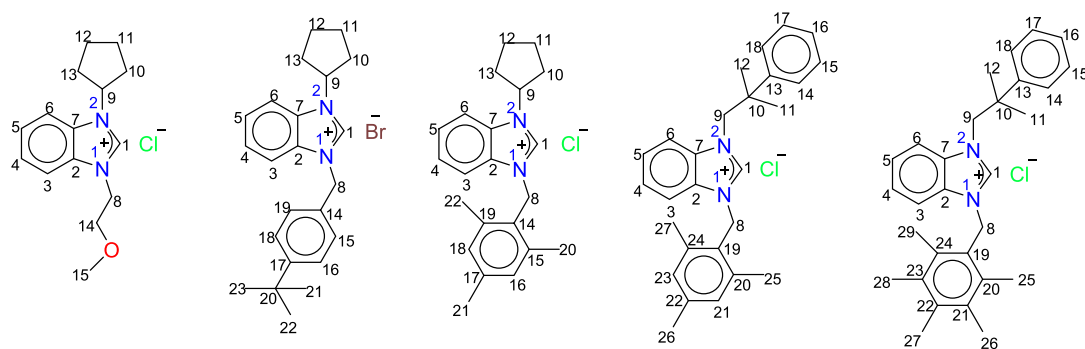
2,4,6-Trimethylbenzyl, X = Cl **HL³(Cl)**

2,3,4,5,6-Pentamethylbenzyl, X = Cl **HL⁵(Cl)**



1

2



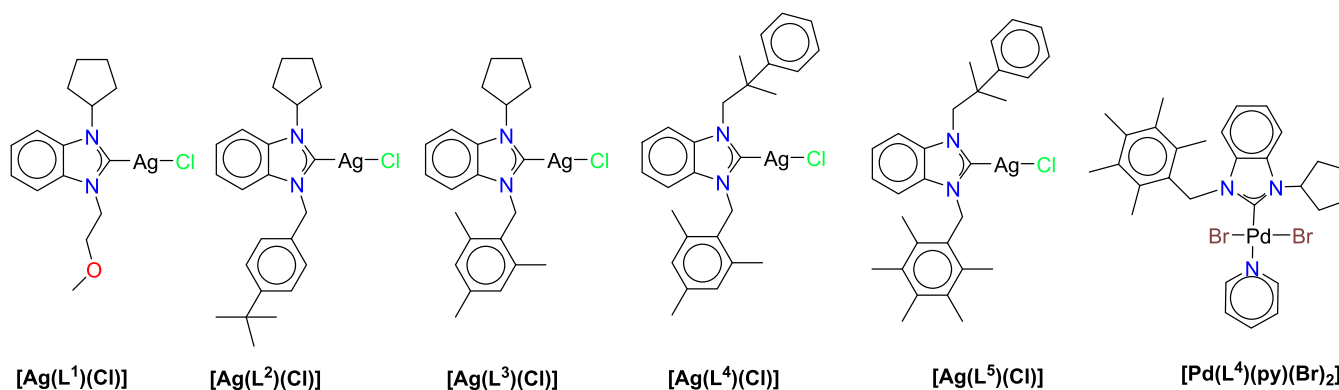
HL¹(Cl)

HL²(Br)

HL³(Cl)

HL⁴(Cl)

HL⁵(Cl)



[Ag(L¹)(Cl)]

[Ag(L²)(Cl)]

[Ag(L³)(Cl)]

[Ag(L⁴)(Cl)]

[Ag(L⁵)(Cl)]

[Pd(L⁴)(py)(Br)₂]

ruthenium(II), palladium(II), zinc(II), and Cd (II) ions.^{7–11} Since then, Pt-based anticancer drugs have been ruling in chemotherapy with the addition of carboplatin and oxaliplatin. However, their limited specificity and escalating resistance have substantially lowered their biomedical utility thus catalyzing the research efforts amid at developing more efficient drugs.¹² Consequently, novel metallodrugs are emerging as potential candidates, via opting for alternative mechanisms of action as compared to conventional platinum-

based drugs, barely interfering in DNA replication and transcription. The novel metallodrugs exhibit significant structural diversity characterized by variations in metal type and oxidation states such as silver(I).^{13–15} These drugs also feature a wide array of redox ligands including N-heterocyclic carbenes (NHCs), pyridylidenes (PYAs),^{16,17} phosphines,¹⁸ and dithiocarbamates.^{19,20}

Silver complexes have long been known as promising contenders due to their therapeutic actions.^{21–24} Recently,

most cancer-targeting drugs consist of silver metal with a variety of plausible ligand designs to achieve the required mechanism mode, as silver complexes have still not entered into clinical trials. Owing to their multifaceted properties and ability to precise targeting mode for anticancer drugs, silver compounds can interact with DNA through metallization. In addition to this, demand for Ag complexes has arisen due to their low toxicity and ease of synthesis. More precisely, imidazolium-based silver drugs have attained strong binding capabilities between metal and ligand moiety to ensure stable carbene complexes that help in therapeutic action by slowing down the release of silver ions at the target site to enhance drug effect.²⁵ Numerous, silver(I) NHCs have been evaluated as having soft functional substituents on imidazolium nitrogen atoms as robust electron reservoirs to offer stability. It can intercalate between DNA base pairs via electrostatic binding.^{26,27}

Pharmacological outcomes of various benzimidazole-functionalized silver-NHCs have remained understudied. Taking this into account, this study reports benzimidazole-based silver complexes with various neutralizing NHC scaffolds to underscore the effect of ligands on silver ions and their contribution to their biological activities. N-arylation of these complexes further assisted in the stability and activity of these complexes. The anticancer activity of the BNHCs proligands was also examined. Molecular docking analysis and density functional theory (DFT) studies were carried out to get insight into the synergistic effect of carbene responsible for the profound activity of silver complexes toward MCF-7 and T47D cell lines. It may depend on the nature and lipophilicity of the ligand and extensive back bonding of the silver carbene bond.

2. RESULTS AND DISCUSSION

The precursors for proligands were synthesized by treating one equivalent of cyclopentyl bromide and (2-chloro-2-methylpropyl) benzene with benzimidazole to yield **1** and **2** as shown in Scheme 1.²⁸ **1** and **2** were further utilized under inert conditions to obtain the NHC proligands ($[\text{Ag}(\text{L}^1)(\text{Cl})]$ – $[\text{Ag}(\text{L}^5)(\text{Cl})]$) by following the reported procedure³⁰ with optimized reaction time and medium. The precursors underwent N-arylation upon adding various aryl halides (R-X) in toluene upon reflux, producing proligands. All of the synthesized compounds were characterized by ¹H, ¹³C, and COSY NMR, IR, HR ESI-TOF mass, and single-crystal X-ray diffraction (XRD) techniques. The carbene proton (C1) peaks in the proligands were observed at around 11.63 and 10.18 ppm in deuterated chloroform. The aromatic protons were observed in the range 7.30–6.84 ppm on both N-substituents of benzimidazole. The N-substituted saturated cyclopentyl group has nine protons at the upfield region, exhibiting some symmetry. Due to puckering and ring strain, they are not equivalent and experience different chemical environments. The methine proton of cyclopentyl group (C9-H) in compounds $\text{HL}^1(\text{Cl})$ – $\text{HL}^3(\text{Cl})$ directly attached to imidazolium nitrogen showed high chemical shift values in the range of 5.05–5.08 ppm as pentet. The remaining protons (C10–C13) were observed as multiplets and stretched between 2.48 and 1.86 ppm. The methoxy-coupled methylene protons in $\text{HL}^1(\text{Cl})$ being electron-donating as compared to 2,4,6-trimethylphenylene substituents attached to C8 in $\text{HL}^3(\text{Cl})$ influenced the chemical shift values of imidazolium protons to upfield region. The carbene proton (C1-H) of $\text{HL}^1(\text{Cl})$

appeared in a more shielded region (11.63 ppm) as compared to $\text{HL}^2(\text{Br})$ and $\text{HL}^3(\text{Cl})$ (12.08–12.07 ppm). A similar trend was observed for aromatic and aliphatic protons, i.e., a slight decrease in the chemical shifts for $\text{HL}^1(\text{Cl})$ as compared to $\text{HL}^2(\text{Br})$ – $\text{HL}^3(\text{Cl})$ except the C1-H proton along with other aromatic and aliphatic protons appeared at the upfield region in $\text{HL}^4(\text{Cl})$.

The complexation occurred under dark conditions in dichloromethane using silver oxide. Silver was coordinated to *in situ* generated free carbene (L^1 – L^5) on stirring as silver oxide acted as a base to deprotonate the proligand and as a metal source. The dark condition was used to avoid the formation of metallic silver and the corresponding side reactions related to photodegradation. The complexes were obtained as a colorless or light-colored powder with excellent yields and were stable under air and moisture. The metalation was confirmed by the disappearance of carbene proton signal (C1-H) around 12.08–10.18 ppm and slight upfield shifting of aromatic protons in complexes were observed. In complexes $[\text{Ag}(\text{L}^1)(\text{Cl})]$ – $[\text{Ag}(\text{L}^3)(\text{Cl})]$, the cyclopentyl proton (C9-H) directly attached with imidazolium nitrogen appeared in the deshielded region with higher chemical shift values at 5.27–5.25 ppm; however, remaining protons of the cyclopentyl moiety were shielded and appeared in the range of 2.28–1.82 ppm as compared to proligands. The same trend was observed in aromatic and aliphatic protons.

In ¹³C NMR spectra, carbene carbon (C1) of proligands appeared at 144.6 ppm and was shifted to the upfield region (135.2–139.5) ppm in complexes. All other aromatic and aliphatic carbon signals were slightly shielded in complexes as compared to proligands. The important functional groups with associated wavenumbers (cm^{-1}) are identified and reported. In the case of the proligand ($\text{HL}^1(\text{Cl})$), a broad signal of the O–H bond was observed at 3383 cm^{-1} . The methoxy ($-\text{OCH}_3$) group was indicated by $\nu(\text{CH})$ and $\nu(-\text{O}-\text{C})$ at 2861 and 1115 cm^{-1} , respectively. However, aromatic and aliphatic C–H peaks were observed around 3100–2900 cm^{-1} in all proligands. In complexes $[\text{Ag}(\text{L}^1)(\text{Cl})]$ – $[\text{Ag}(\text{L}^5)(\text{Cl})]$, a minor reduction in peak frequencies was seen in aromatic and aliphatic C–H stretching signals. Moreover, C=N stretching vibrations of imine were found in the range 1665–1625 cm^{-1} in all compounds. However, signals around 1480–1387 cm^{-1} showed C–N bending and C–C stretching of compounds. Meanwhile, silver carbene signals are usually observed in fingerprint regions around 544–566 cm^{-1} with very low intensity.

The electrospray ionization high-resolution time-of-flight mass spectrometry (HR ESI-TOF MS) (+) was operated in dichloromethane, and the low-intensity molecular ion peak was in agreement with $[\text{M} - \text{Cl}]^+$ in all compounds. There is a conspicuous match between calculated and observed MS spectra in all compounds.

2.1. X-ray Crystallographic Analysis. The single crystal of suitable diffraction quality for **1**, $\text{HL}^2(\text{Br})$ and $[\text{Ag}(\text{L}^3)(\text{Cl})]$ were obtained by a layering method using their dichloromethane solution (5 mL) with ether (1 mL) at room temperature and their oak ridge thermal ellipsoid plot (ORTEPs) are shown in Figures 1–3. The colorless crystals were obtained, followed by washing with ether and drying in air. The crystal structure of $[\text{Ag}(\text{L}^3)(\text{Cl})]$ reveals the formation of a dimer with two silver atoms bridged by chloride moiety. The two L^3 ligands are aligned in *trans* configuration around silver forming a four-membered ring structure with chlorides

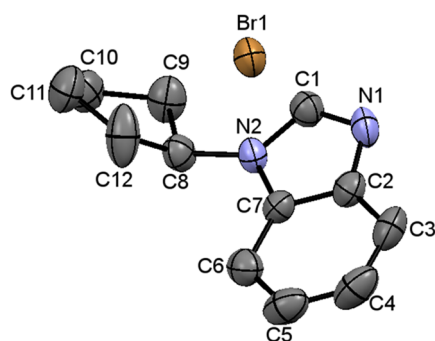


Figure 1. ORTEP view of the molecular structure of **1**. Ellipsoids are drawn at the 20% probability level; hydrogens have been omitted for clarity.

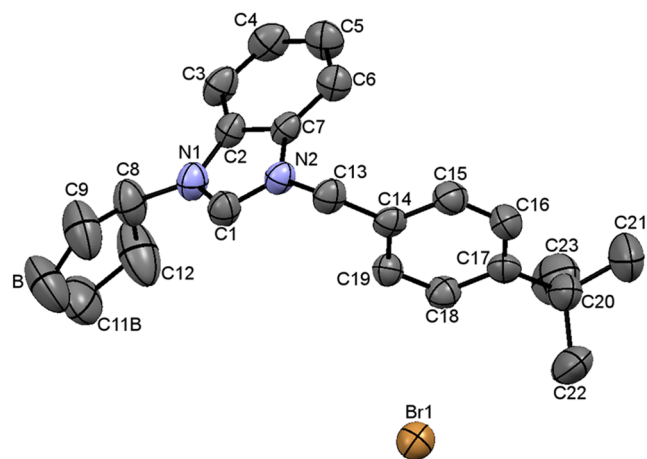


Figure 2. ORTEP view of the molecular structure of **HL²(Br)**. Ellipsoids are drawn at the 20% probability level; hydrogens have been omitted for the sake of clarity.

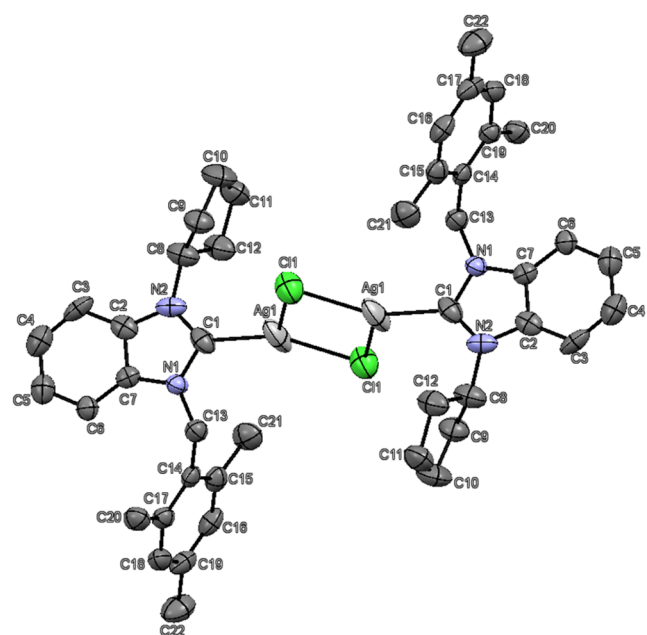


Figure 3. ORTEP view of the molecular structure of **[Ag(L³)(Cl)]**.

(Ag₂Cl₂), making it noteworthy in terms of stability and reactivity. The packing diagram of complex **[Ag(L³)(Cl)]** is shown in Figure S30. It reveals no van der Waals or π - π

interactions present in the crystal lattice. There is also a lack of hydrogen bonding, and pure compounds are obtained without any trapped solvent moieties. Important bond lengths and bond angles of complex **[Ag(L³)(Cl)]** are given in Table 1. While important bond lengths and angles of **1**, **HL²(Br)** are shown in Tables S1 and S2.

Table 1. Selected Structural Parameters of **[Ag(L³)(Cl)]**

bond lengths (deg)		bond angle (Å)	
C1–N2	1.33(1)	C8–N2–C1	126.4(7)
Ag1–C1	2.108(6)	N2–C1–Ag1	132.9(6)
Ag1–Cl1	2.730(2)	C1 Ag1 Cl1	115.3(2)
Ag1–Cl1	2.421(2)	C13 N1 C1	125.2(6)
C1–N1	1.36(1)	N1 C1 Ag1	120.7(5)

Ellipsoids are drawn at the 20% probability level; Hydrogens have been omitted for clarity.

2.2. DNA Binding Studies. The anticancer drug effectiveness is also based on the mechanism of its binding mode, chemical character, and selectivity with DNA. The binding of DNA with potent compounds can be studied by absorption spectroscopy, which correlates with electronic modifications. These spectral alterations are related to the determination of binding constants and help assess the attachment site. In this study, the most active cytotoxic silver complex **[Ag(L⁴)(Cl)]** (**10**) and its proligand **HL⁴(Cl)** (**5**) were used to study the drug–DNA interactions by using spectroscopic method. To analyze their behavior, absorption spectra were recorded with/without the presence of CT-DNA.^{29,30} The CT-DNA concentration was measured using extinction coefficient at 260 nm ($\epsilon = 6600 \text{ M}^{-1} \text{ cm}^{-1}$) to prepare the stock solution and make sure that CT-DNA is free of proteins.³¹ The absorption spectra were recorded while maintaining a constant drug concentration of 4 μM and varying the amount of CT-DNA from 1 to 7 μM gradually. The UV–vis maxima of compounds 270 and 279 nm for (**5**) and 274 and 279 nm for complex (**10**) can be attributed to π - π^* transition (see Figure 4).

In the case of **HL⁴(Cl)**, a hypochromic shift (decrease in absorption values) was observed, leading to the intercalative DNA interactions with proligand causing the unwinding of the double helix *via* disrupting the base pairs. Stacking interactions involve electronic transitions (π electrons) among ligands and DNA molecules. Furthermore, in compound (**10**) hyperchromic effect (increase in absorption) was observed evident from the UV-spectrum due to the presence of possible electrostatic interaction between the silver cation and the negatively charged phosphate group of DNA, thereby instigating the disruption of the DNA secondary structure.^{32,33} This effect can be attributed to external contact³⁴ without significant changes in absorption spectrum as a result of weaker interaction among DNA and complex.

The association constant values (K_b) quantify the strength of the binding capabilities of compounds with DNA. The binding constant values were attained in the range of 7.20 – $6.06 \times 10^4 \text{ M}^{-1}$ using the slope-to-intercept ratio method. It was computed using $A_0/(A - A_0)$ vs $1/[\text{DNA}]$ formula.^{35,36} The Gibbs free energy of the compound–DNA adduct was calculated by using K_b values following this formula ($G = -RT \ln K_b$). The calculated values are shown in Table 2 and inset graphs are shown in Figure 4. The negative free energy associated with the binding of compounds indicated the

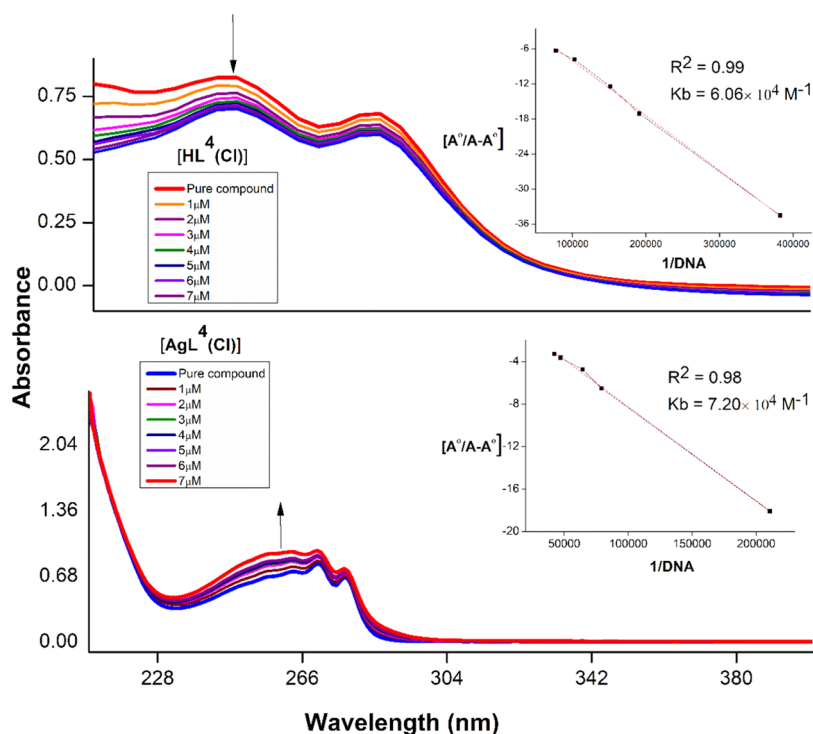


Figure 4. Changes in UV–Vis absorption spectra of $[\text{Ag}(\text{L}^4)(\text{Cl})]$ and $\text{HL}^4(\text{Cl})$ in the presence and absence of CT-DNA in a Tris-HCl buffer system of pH 7.4. The black arrow indicates the changes in absorbance on increasing the concentration of DNA.

Table 2. UV–Vis Spectral Data of the Interaction with CT-DNA

compound	λ_{max} (nm)	$(\Delta A/A_0)$ (%)	$K_b \times 10^4$ (M^{-1})	ΔG° (kcal/mol)
$[\text{Ag}(\text{L}^4)(\text{Cl})]^a$	274	(−8.6)	7.20	−8.94
$\text{HL}^4(\text{Cl})^b$	270	(−6.7)	6.06	−7.26

^aShows hyperchromism. ^bShows hypochromism.

spontaneity of reactions.³⁷ The k_b values are higher in the case of complex **10** relative to its ligand (**5**) which indicates the strong interaction of the complex with DNA as compared to a ligand that exhibits mild binding interaction.

2.3. DNA Binding Studies Using Cyclic Voltammetry.

Cyclic voltammetry (CV) is a powerful tool to determine the electrochemical responses in the form of current produced by varying potential to investigate the binding interactions of DNA. This technique further assists in determining a compound as a potential drug contestant.^{38,39} Electrochemical measurements were carried out in conventional three-electrode systems such as Ag/AgCl as reference electrode, glassy carbon as working electrode (GCE-2 mm), and Pt wire as auxiliary electrode. The sample solutions of $[\text{Ag}(\text{L}^4)(\text{Cl})]$ (**10**) and $\text{HL}^4(\text{Cl})$ (**5**) (0.01 mM) were prepared in DMF/TBAPF₆ (5 mL/0.1 M). All of the measurements were taken under an inert environment (N_2) by purging nitrogen for 20 min before every measurement to remove oxygen involvement. Stock solution (Tris-HCl buffer system of pH 7.4) of CT-DNA was used to record measurements while a 100 mV s^{-1} scan rate was maintained throughout the experiment. A potential window was selected as −2.0 to +1.8 V vs Ag/AgCl to record the electrochemical response of compounds. First, the CV of the sample solution (compound + TBAPF₆) was referred to as a blank experiment (black curve in Figure 5). A few key findings were observed from the cyclic voltammetry curves of

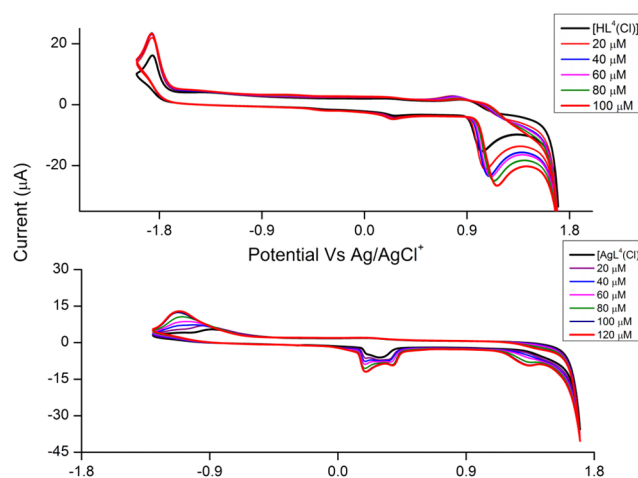


Figure 5. Changes in cyclic voltammograms of $[\text{Ag}(\text{L}^4)(\text{Cl})]$ and its respective ligand $\text{HL}^4(\text{Cl})$ in the presence and absence of CT-DNA in a Tris-HCl buffer system at pH 7.4.

$[\text{Ag}(\text{L}^4)(\text{Cl})]$ and $\text{HL}^4(\text{Cl})$. In the case of proligands (**5**) voltammograms showed redox behavior; oxidation peak ($E_{\text{pa}1/2}$) appeared at 0.95 V while reduction peak potential ($E_{\text{pc}1/2}$) was observed at −1.77 V vs Ag/AgCl. This can be associated with ligand oxidation and reduction during electrolysis. Calf thymus DNA was added incrementally (20–120 μM) during electrochemical measurements, and spectra were recorded after every addition. The changes in the CV profile of the compound recommended binding potential with DNA and were evident from a positive shift in $E_{\text{pa}1/2}$ (1.06 V) with an appreciable increase in anodic peak current (I_{pa}). As CT-DNA concentration increased, cathodic peak current (I_{pc}) enhanced, but there was no change in cathodic peak potential (−1.77 V). An appreciable change in positive peak potential

suggests that proligands are showing an intercalation mode of interaction. Carter and Bard also reported that a positive shift in peak potential would lead to intercalative mode.⁴⁰

Similarly, in $[\text{Ag}(\text{L}^4)(\text{Cl})]$ one cathodic peak observed at -0.75 V while one broad anodic peak was appeared at 0.36 V.⁴¹ After adding CT-DNA, spectra were recorded, and a clear increment in peak currents (I_{pc} or I_{pa}) was observed, indicating the silver complex's interaction with CT-DNA. Furthermore, an anodic peak shoulder emerged at a more negative potential (0.25 V) during measurement along with a shift in peak potential ($E_{\text{pa1/2}} = 0.41$ V) (Figure 5). The redox behavior of complex⁴² was confirmed from CT-DNA-Ag(I) electrochemical response.⁴³

This type of cyclic voltammogram response of silver(I) complexes has been reported in the literature ($\text{Ag}^0 \leftrightarrow \text{Ag}^+ + \text{e}$).^{44,45} It usually arose due to a slow diffusion process upon complex-CT-DNA binding via an electrostatic mode of interactions between positively charged metal ions and negatively charged phosphate groups of DNA. This technique is also useful in determining the diffusion rate and kinetics of the compound-DNA interaction. The mentioned silver complex (**10**), $[\text{Ag}(\text{L}^4)(\text{Cl})]$, responded strongly toward cancerous cells (Table 6) and also justified strong CT-DNA interactions (as shown in this section and Table 2).⁴⁶

Hydrodynamic techniques offer a reliable approach for evaluating binding models of compounds in solution form and are highly sensitive to changes in structures. Viscosity measurement is one of these techniques which provides a clear indication of structural changes in DNA.⁴⁷ This technique also distinguishes between intercalative and electrostatic binding modes, providing an experimental framework to analyze the DNA–compound interactions. Specifically, in the intercalative binding mode, there must be an appreciable increase in viscosity.⁴⁸ While in electrostatic binding mode, there is minimal or no effect on solution viscosity was reported.⁴⁹ In the case of $\text{HL}^4(\text{Cl})$, an increase in solution viscosity with a gradual increase in compound concentration was observed which is indicative of intercalation binding mode, shown in Figure 6. This behavior emerged due to the lengthening and stiffening of DNA upon insertion of the

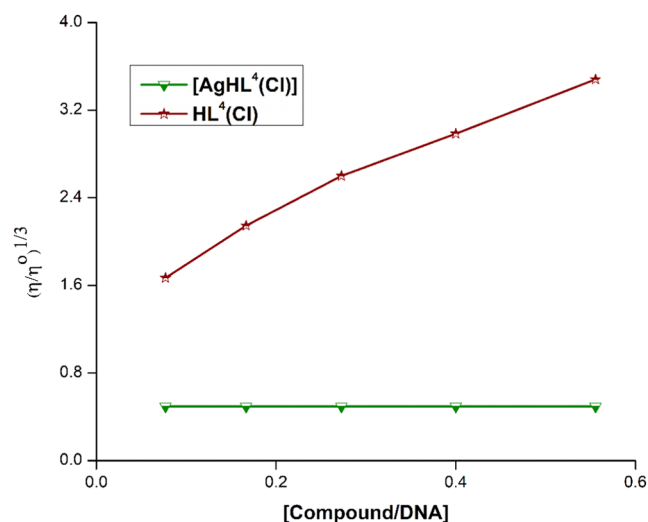


Figure 6. Relative viscosity $(\eta/\eta^0)^{1/3}$ of CT-DNA in the absence and presence of increasing amounts of $[\text{Ag}(\text{L}^4)(\text{Cl})]$ and $\text{HL}^4(\text{Cl})$.

compound into its base pairs, thereby increasing the viscosity. In complex $[\text{Ag}(\text{L}^4)(\text{Cl})]$, electrostatic interaction between the negatively charged DNA backbone and the silver complex was indicated by no change or minimal effect on solution viscosity upon increasing complex concentration (Figure 6).

There are many ways to check the stability of complexes in solution phase like NMR, UV–vis spectroscopy, and MS spectrometry.⁵⁰ In this study, the stability of $[\text{Ag}(\text{L}^4)(\text{Cl})]$ (**10**) was monitored under physiological conditions using phosphate-buffered saline (PBS) (0.1 M, $\text{pH } 7.4$) and Tris-HCl buffer system by UV–vis spectroscopy. The solution of compound **10** (0.1 mg L^{-1}) was prepared in a DMSO/buffer system using a small amount of DMSO (10%) to completely dissolve the **10** and spectra were recorded using a UV-3600 Shimadzu. The time-dependent spectrum was recorded at room temperature for representative complex **10** to highlight its stability in an alkaline medium using PBS and a Tris-HCl system at various time intervals. PBS was added gradually from 100 to $1000 \mu\text{L}$ and spectrum was taken. The sample was reserved after the final addition ($1000 \mu\text{L}$), and spectra were recorded for various time intervals from 5 min to 72 h (Figure 7). In another case, sample **10** was freshly prepared in a Tris-

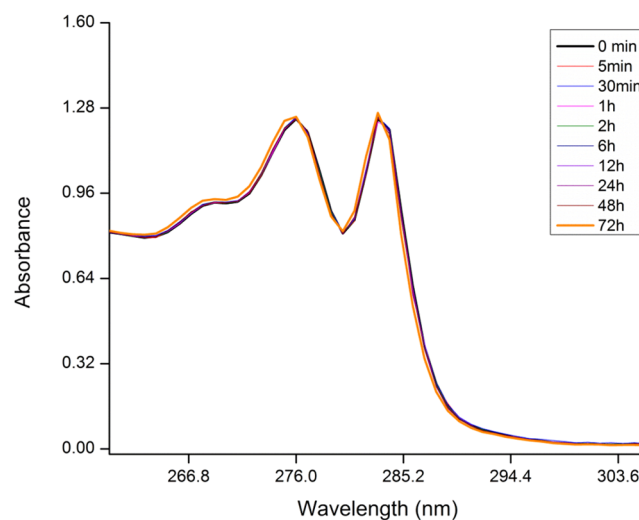


Figure 7. Stability studies of $[\text{Ag}(\text{L}^4)(\text{Cl})]$ in phosphate-buffered saline (PBS) at $100\text{--}1000 \mu\text{L}$ ($\text{pH } 7.4$, 0.1 M) under UV–vis NIR (UV-3600) in 72 h.

HCl buffer, and spectra were recorded. The sample was then preserved, and spectra were taken after various time intervals (Figure S31). The repetitive response without any extra peak and constant spectral pattern over the studied course of time assured the stability of the complex under physiological conditions. The stability of complexes is a crucial factor in determining the effectiveness of a drug under biological environments. The stable complexes remained intact and active until they reached their target site. Furthermore, solution stability and degree of solubilization in buffer systems also provide insights into their bioactivity. A strong sigma donor and π acceptor nature of NHC ligands contribute to the stability of silver complexes in solution form. These complexes remained undegraded while placed in PBS and the solution remained clear, without the formation of black particles or AgCl. In the case of silver nitrate or silver chloride black color, precipitates appeared immediately when placed in buffer solution. The UV–vis response of this solution was observed

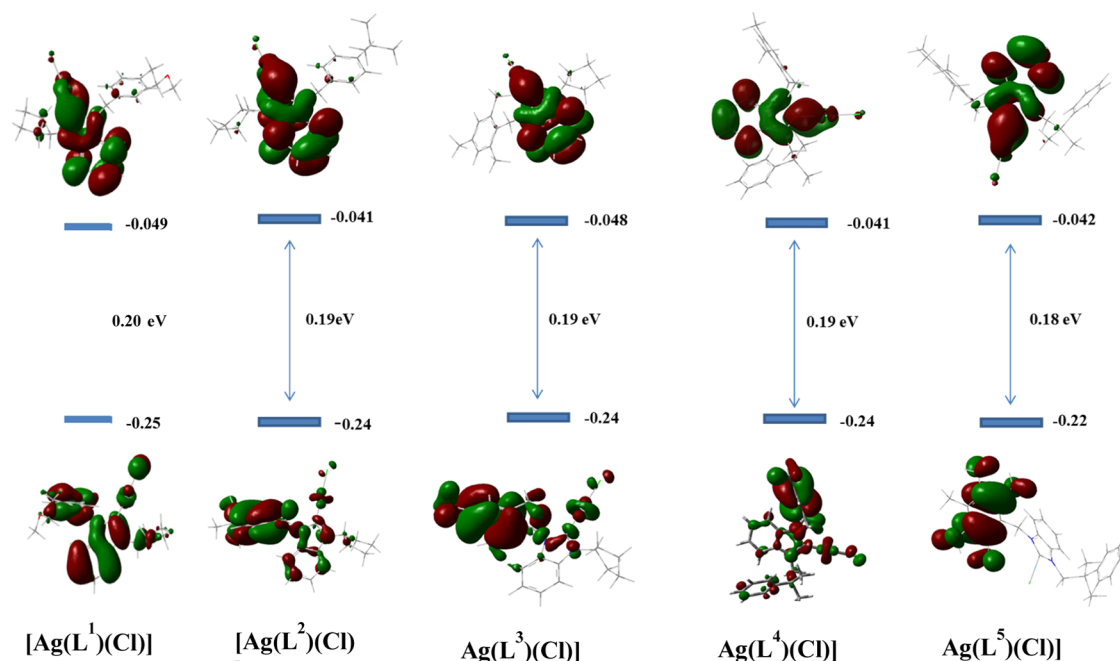


Figure 8. Energy level diagrams of frontier molecular orbitals (HOMO, LUMO) and energy gap (ΔE) for $[\text{Ag}(\text{L}^1)(\text{Cl})]$ – $[\text{Ag}(\text{L}^5)(\text{Cl})]$ complexes.

in the spectrophotometer and curves remained the same before and after adding buffer solution which showed the stability of complexes over various time intervals (72 h). In addition, silver complexes' stability can be explained based on their solubility in aqueous systems. The silver NHC complexes are moderately soluble in an aqueous solution (95:5 water:DMSO) and therefore, remain intact in PBS compared to silver nitrate which is highly soluble in an aqueous medium.⁵¹ However, side chains (alkyl or aryl substituents) also play a role in the steric bulkiness of complexes, affecting their stability in solution.

2.4. DFT Calculations and Optical Properties. The geometries of complexes were designed by Gaussview 09 software and optimized using the Gaussview 16 program.⁵² For optimization, effective core potential B3LYP/LANL2DZ method⁵³ was adopted for silver complexes with 6-31-G** basic set for all other atoms (H, O, C, N).⁵⁴ The ground states of complexes were optimized in acetonitrile using the PCM (Polarizable Continuum Model) method. In addition, the LANL2DZ basis set has relativistic effects, and suitable for metal ions, and is widely employed in DFT calculations.⁵⁵ Energy gap (ΔE), electronegativity (χ), absolute hardness (η), chemical potential (μ), absolute softness (σ), and global electrophilicity (ω) were calculated by using eqs 1–7 presented in Table S3. The electronic properties of compounds provide valuable insights into their biological actions. Highest-occupied molecular orbital–lowest-unoccupied molecular orbital (HOMO–LUMO) gap (ΔE) is a key parameter in the design of compounds as it is directly related to electron transfer processes during compound–target interactions (Figure 8). The LUMO of the compound should be close in energy with the HOMO of biological targets to smoothen the electron transfer process leading to the generation of reactive intermediates such as reactive oxygen species (ROS) that hits cancerous cells and ensures therapeutic efficacy.⁵⁶ Furthermore, molecular electrostatic potential (MEP) surfaces provide insights into potential reactive sites on silver complexes during interactions (Figure S32). Generally, blue colors represent the negative potential sites

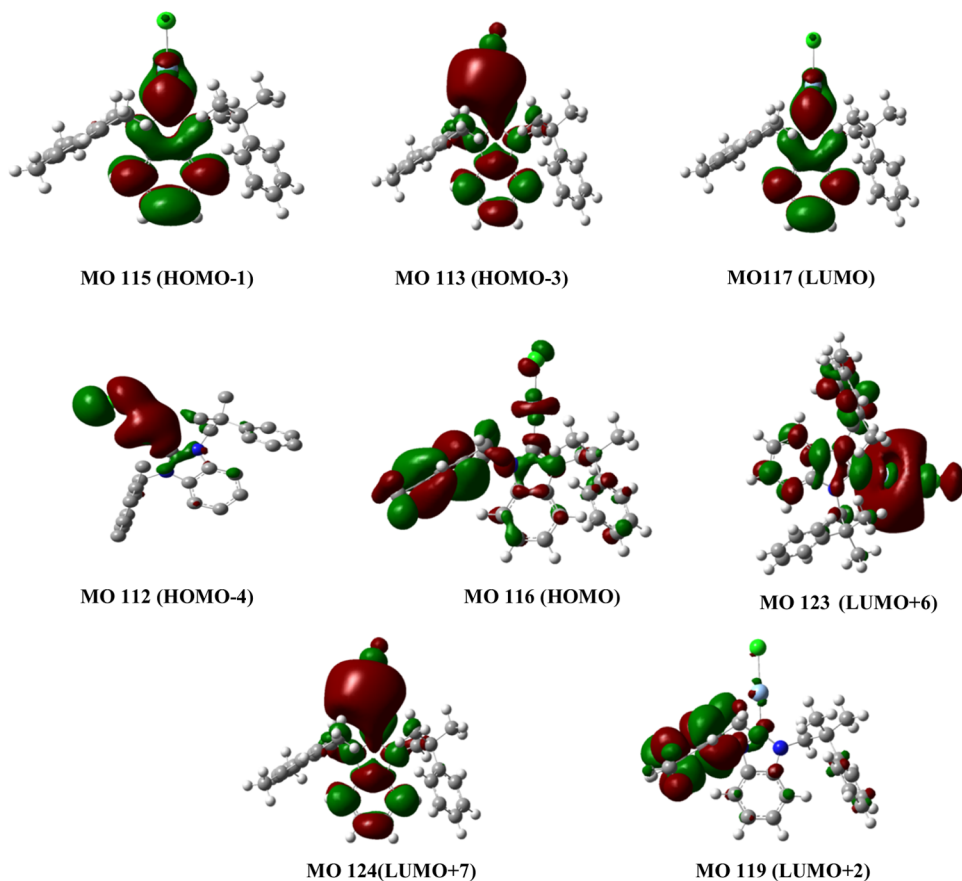
while red color shows nucleophilic sites.⁵⁶ The drug molecules that have high electropositive surfaces exhibit high binding affinities for electronegative surfaces of DNA, thereby crucial in selective binding.

χ (Chi) represents the electronic response or susceptibility of a compound to external perturbations. Moreover, its higher values can be associated with the higher dielectric properties of complexes, which in turn gives insight into compound reactivities. It also quantifies the electron-donating and -accepting natures of ligands. Low chi values (0.148–0.143) were found in all complexes due to the strong sigma donor and back bonding nature of NHC ligands. An exception was found in $[\text{Ag}(\text{L}^5)(\text{Cl})]$, this is probably due to the steric bulkiness around silver metal which hinders the effective back-donation of electrons, hence strong sigma character was there.^{57,58} η (Eta) is known as chemical hardness, which indicates the greater resistance toward electronic distribution. Its higher values signify the stability of the chemical species. The η values were calculated in the range of 0.099–0.089 for all complexes which indicates the soft nature of complexes (see Table S3). In addition to this, higher polarizability leads to better reactivity due to changes in electronic environment. σ (Sigma) exchange-correlation potential or energy is a key component in DFT calculation. It is used to predict the electronic properties of compounds such as energy bands and magnetic and chemical properties. It also explains the correlation of electrons among the compounds. Its lower values in all complexes were found in DFT calculation, which indicated the strong bonding interaction among electron-rich regions. Π (Pi) is important in DFT calculations for understanding bonding, conjugation, and back-donation. Specifically, low values were observed in all complexes ranging from -0.148 to -0.136 that validated the concept of strong sigma donor and poor Π acceptor nature of NHC ligands (see Table S3). ω (Omega), known as the global electrophilicity index, is used to study the different excited states of compounds. It also tells us about the electrophilic nature of the complexes. In the present study, all complexes

Table 3. Molecular Orbitals and Their Oscillator Strength with % Contribution^a

MO115 → MO117, $f = 0.54924$ (68.82%)	MO115 → MO117, $f = 0.54924$ (68.82%)
MO113 → MO117: $f = 0.51817$ (59.534%)	MO113 → MO117: $f = 0.51817$ (59.534%)
MO116 → MO119: $f = 0.51180$ (65.133%)	MO116 → MO119: $f = 0.51180$ (65.133%)
MO112 → MO123: $f = 0.39913$ (35.364%)	MO112 → MO123: $f = 0.39913$ (35.364%)
MO116 → MO124: $f = 0.39692$ (42.904%)	MO116 → MO124: $f = 0.39692$ (42.904%)

^aMO = molecular orbital, f = oscillator strength, tells us about absorption intensities.

Figure 9. Pictorial representation of contributing molecular orbitals ($\pi \rightarrow \pi^*$ transitions) in absorption maxima.

showed very low electrophilicity values due to the strong sigma donor and π acceptor natures of NHC ligands.

$$P_i = -\chi \quad (1)$$

$$\sigma = 1/\eta \quad (2)$$

$$\Delta E = E_{\text{LUMO}} - E_{\text{HOMO}} \quad (3)$$

$$\omega = \frac{P_i^2}{2\eta} \quad (4)$$

$$\eta = \frac{E_{\text{LUMO}} - E_{\text{HOMO}}}{2} \quad (5)$$

$$\Delta E = E_{\text{LUMO}} - E_{\text{HOMO}} \quad (6)$$

$$\chi = \frac{-(E_{\text{HOMO}} + E_{\text{LUMO}})}{2} \quad (7)$$

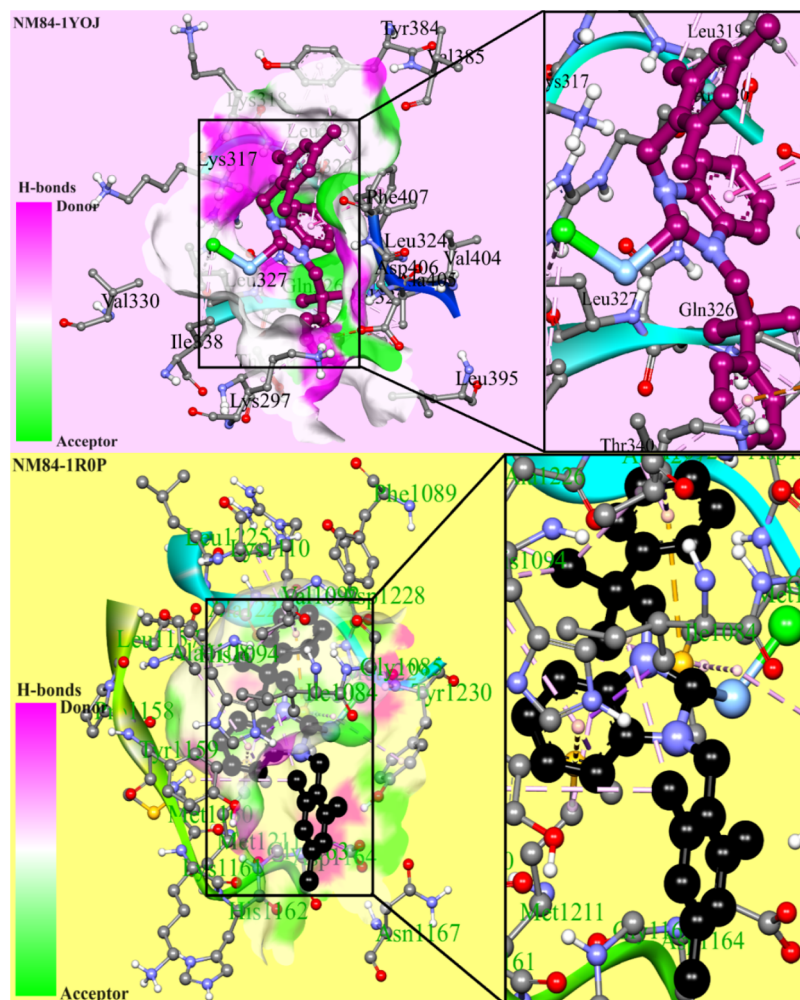
In this present study, time-dependent DFT (TD-DFT) calculations⁵⁹ were carried out to foresight various optical parameters of compounds ([Ag(L¹)(Cl)]-[Ag(L⁵)(Cl)]). The calculated UV spectra of the complex (10) are shown in Figure

S33 and compared with the experimentally calculated spectrum (see Figure S34). The molecular orbitals responsible for maximum absorption wavelengths and oscillator strength are mentioned below. In both spectra, absorption maxima lie in the UV region, whereas the difference in peak maxima is due to different mediums. In the case of theoretical calculations, acetonitrile was used, while in the case of experimental spectra, Tris-HCl buffer with 10% DMSO was used. A few weak absorption bands correspond to metal-to-ligand charge transfer (MLCT) neat 300–400 nm observed in [Ag(L⁵)(Cl)] mainly responsible for HOMO → LUMO transitions. The contributing MO (molecular orbitals) to maximum absorption with oscillator strength is enlisted in Table 3, and their pictorial forms are listed in Figure 9.

2.5. Molecular Docking. Molecular docking studies are essential to forecast and examine the interactions between putative therapeutic candidates and their biological targets for the drug discovery process.⁶⁰ Determining the binding affinity and specificity offers comprehensive insights into the mode of action of a molecule.⁶¹ Molecular docking speeds up identifying potential lead compounds by mimicking these

Table 4. Ligand–Protein Binding Energies and Ligand Efficiencies (LE) of the Docked Molecules with EGFR, VEGFR2, FGFR, SRC, and HGFR Substrates

compounds	binding energy/LE					
	EGFR SWB7	EGFR 1M17	VEGFR2 2XIR	FGFR 4QQT	SRC 1YOJ	HGFR 1R0P
[Ag(L ¹)(Cl)]	−5.13/−0.26	−5.89/−0.29	−6.65/−0.33	−6.25/−0.31	−5.95/−0.30	−6.95/−0.35
[Ag(L ²)(Cl)]	−7.63/−0.26	−8.13/−0.28	−8.49/−0.29	−7.90/−0.27	−7.93/−0.27	−8.98/−0.31
[Ag(L ³)(Cl)]	−6.41/−0.25	−7.96/−0.31	−7.59/−0.29	−7.74/−0.30	−6.97/−0.27	−8.25/−0.32
[Ag(L ⁴)(Cl)]	−6.25/−0.2	−7.39/−0.24	−7.17/−0.23	−7.78/−0.25	−7.34/−0.24	−8.47/−0.27
[Ag(L ⁵)(Cl)]	−6.24/−0.19	−7.88/−0.24	−7.88/−0.24	−8.09/−0.25	−7.05/−0.21	−8.78/−0.27
Tamoxifen	−6.07/−0.22	−8.26/−0.29	−7.65/−0.27	−7.52/−0.27	−6.83/−0.24	−8.53/−0.30

**Figure 10.** Three-dimensional depictions of docked complexes representing the interactions of complex [Ag(L⁴)(Cl)] in the binding pocket of target SRC (pink background) and HGFR (yellow background) proteins.

interactions and refining their design before synthesis and experimental testing.⁶² The results in Table 4 represent the binding energies and ligand efficiencies of the synthesized candidates [Ag(L¹)(Cl)], [Ag(L²)(Cl)], [Ag(L³)(Cl)], [Ag(L⁴)(Cl)], and [Ag(L⁵)(Cl)], thus comparing the relative strengths of binding and their effectiveness as inhibitors of the screened cancer proteins. The binding energy and compound efficiency values collectively decide the best target substrate for a compound, and the computational outcomes will align with the in vitro results. In the present study, two crystal structures of EGFR (epidermal growth factor receptor) are type I receptors of the tyrosine kinase (TK) family, and a crystal

structure for each of the VEGFR2 (vascular endothelial growth factor receptors), FGFR (fibroblast growth factor receptor), and SRC (proto-oncogene tyrosine kinase protein) also known as nonreceptor tyrosine kinase protein, and HGFR (hepatocyte growth factor receptor) is a part of MET gene, were selected for docking investigations, and the results were compared with a binding capability of tamoxifen used as a reference for the in vitro studies. From the achieved results, only compound [Ag(L¹)(Cl)] was bound with an EGFR protein with greater binding energy than tamoxifen, the compounds [Ag(L²)(Cl)] and [Ag(L⁴)(Cl)] were potent against VEGFR2, and the compounds [Ag(L¹)(Cl)], [Ag(L³)(Cl)], [Ag(L⁴)(Cl)], and

[Ag(L⁵)(Cl)] were strongly bound with FGFR. However, the parameters deciding the potential of a complex to bind with its target substrate include binding energies and complex efficacies which were found better with the SRC and HGFR proteins and were selected for further two- and three-dimensional binding interaction analyses of screened motifs shown in Figure 10.

An analysis of the protein-complexes of the screened motifs against the SRC target substrate revealed that all of the complex molecules occupied the same binding pocket of the protein in each complex with the amino acids Lys B:297, Lys B:317, Lys B:318, Leu B:319, Arg B:320, His B:321, Leu B:324, Val B:325, Gln B:326, Leu B:327, Val B:330, Ile B:338, Thr B:340, Tyr B:384, Val B:385, His B:386, Leu B:395, Val B:404, Ala B:405, Asp B:406, and Phe B:407. It is obvious from the two-dimensional representations of interactions between the complex and the target substrate as shown in Figure 11 that the compound [Ag(L⁴)(Cl)] is forming only the weak van der Waals forces with the amino acid residues,

thus accounting for relatively weaker bindings with a lower binding energy of -7.05 kcal/mol than the ligand HL⁴(Cl) which has the similar structural fragments; however, it formed a strong π -anion force (3.43 Å) with the carboxylate moiety of Asp B:406 amino acid residue. The chlorine atom of [Ag(L⁴)(Cl)] was involved in forming van der Waals forces (4.06 and 4.99 Å) with the alkyl chains of Leu B:327 and Ile B:338 amino acids but these forces were absent in the complex of [Ag(L⁵)(Cl)] (see Figure S35). Moreover, the six-membered carbocyclic ring of the benzimidazole moiety was tightly bound with numerous amino acid residues including Phe B:407 forming a π - π T shaped force, whereas this amino acid was simultaneously bound by a π -alkyl force (4.80 Å) with the *p*-methyl group substituted at the aromatic ring, thus twisting the molecule in V-shaped along with two other π -alkyl forces between the π electrons of the benzimidazole moiety and the alkyl chains of Leu B:319 (5.15 Å) and Leu B:324 (5.18 Å) amino acid residues. In the ligand-protein complex of compound [Ag(L¹)(Cl)] with SRC protein, the amino acid residue Phe B:407 plays a key role in the binding through a hydrogen bond (4.34 Å) with the oxygen atom of the methoxy group and through a van der Waals force (4.50 Å) with the silver atom, whereas another amino acid Lys B:317 constituted a π -cation force (3.94 Å) with the aromatic ring of the ligand molecule (see Figure S35). In conclusion, these binding patterns and binding energies of the screened candidates were found to be in good agreement with experimentally determined anticancer potency.

Considering the complex-protein of compounds [Ag(L⁵)(Cl)], [Ag(L¹)(Cl)], and [Ag(L⁴)(Cl)] against the HGFR target substrate revealed that the ligand occupied the binding pocket bearing the amino acid residues Ile A:1084, Gly A:1085, Arg A:1086, Gly A:1087, His A:1088, Phe A:1089, Val A:1092, Ala A:1108, Lys A:1110, Leu A:1140, Leu A:1157, Pro A:1158, Tyr A:1159, Met A:1160, Lys A:1161, His A:1162, Gly A:1163, Asp A:1164, Met A:1211, Leu A:1225, Ala A:1226, Arg A:1227, Asp A:1228, Met A:1229, Tyr A:1230, Asp A:1231, and Lys A:1232. According to the behavior of compound [Ag(L⁵)(Cl)] (see Figure S36) expected after performing the in vitro assays, this compound has formed only weak van der Waals forces of interactions with various amino acid residues in the binding pocket of the protein. On the other hand, [Ag(L¹)(Cl)] (see Figure S36) formed a stronger hydrogen bond (1.96 Å) through its oxygen atom with the amidic NH of Tyr A:1230 amino acid. The compound [Ag(L⁴)(Cl)] was binding strongly with the target substrate through a π -sulfur interaction (4.11 Å) between the electronic cloud of the phenyl ring and three π - σ forces (3.75 , 3.96 , and 3.81 Å) with Ile A:1084, Val A:1092, and Met A:1211 amino acid residues, and this compound was also found to be the most potent candidate during in vitro screening.

2.6. Anticancer Properties; Cytotoxic Study. The cytotoxic effects of all compounds (1–11) on the human breast carcinoma cell lines (MCF-7, T47D) and the normal cell line (Vero) were assessed by using the 3-(4,5-dimethylthiazol-2-yl)-2,5-diphenyl-2H-tetrazolium bromide (MTT) assay. The selection of assay was due to its widespread recommendation as a quick and reliable method for evaluating toxicity in cancer cells, as well as its practical availability. In MCF-7 and T47D, inhibition of carcinoma cell growth occurred at IC₅₀ values below 50 μ M after 48 h of treatment for all compounds (Table 5). We also determined the IC₅₀ values for Tamoxifen, which serves as a control drug for breast

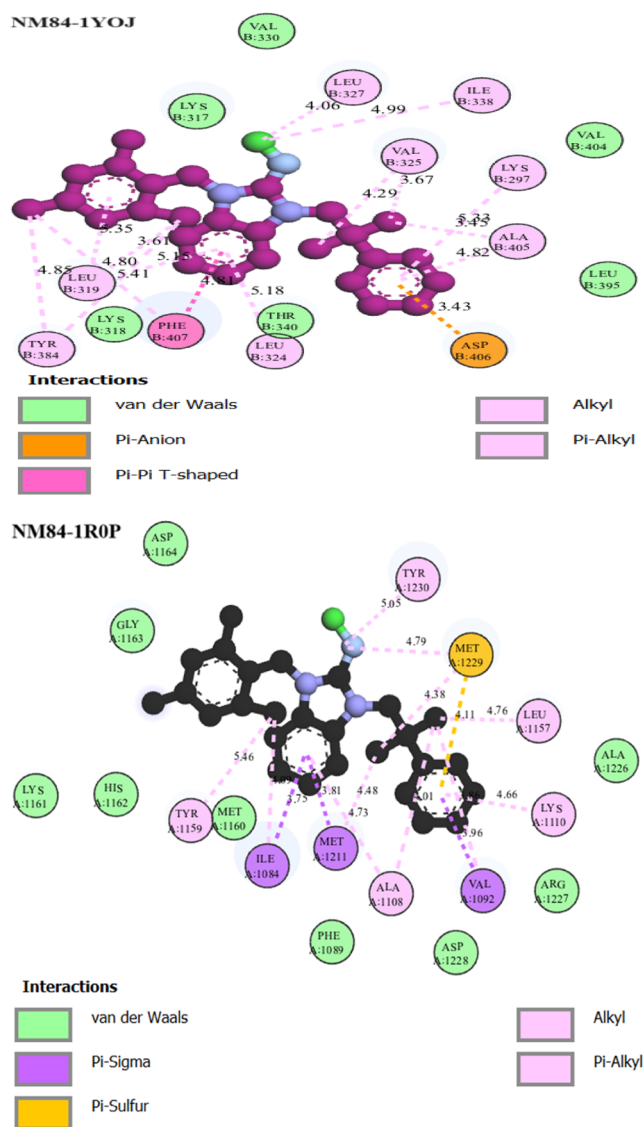


Figure 11. Two-dimensional binding pocket and ligand interaction visualizations of [Ag(L⁴)(Cl)] with the SRC and HGFR target substrates.

Table 5. Cytotoxicity (IC₅₀) of Cancer Cell Lines (μM)^a

#	compounds	codes	MCF-7	T47D
1	1	1	37 ± 1.93	41 ± 2.12
2	HL ¹ (Cl)	2	29 ± 0.76	33 ± 2.12
3	HL ² (Cl)	3	22 ± 1.02	30 ± 1.41
4	HL ³ (Cl)	4	22 ± 1.24	24 ± 0.71
5	HL ⁴ (Cl)	5	16 ± 0.77	31 ± 2.12
6	HL ⁵ (Cl)	6	28 ± 1.73	34 ± 2.12
7	[Ag(L ¹)(Cl)]	7	13 ± 1.17	15 ± 1.41
8	[Ag(L ²)(Cl)]	8	24 ± 0.47	25 ± 2.12
9	[Ag(L ³)(Cl)]	9	16 ± 1.12	18 ± 1.41
10	[Ag(L ⁴)(Cl)]	10	9 ± 1.04	11 ± 1.41
11	[Ag(L ⁵)(Cl)]	11	15 ± 1.07	17 ± 2.12
12	Tamoxifen	Tamoxifen	11 ± 1.34	13 ± 0.71

^aFor statistical analysis, three replicates were treated, and the results were expressed as the mean SEM of two individual values for growth inhibition percentages. Using “GraphPad” Prism 9 “GraphPad”, (“San Diego” California), a “nonlinear regression model” (curve-fit) based on a “sigmoidal dose-response curve” (variable) was created to get the IC₅₀ value for cytotoxicity.

cancer cells. According to these IC₅₀ values, MCF-7 appeared to be more sensitive to the treatment than T47D.

Compounds from precursor (1) to proligands, HL¹(Cl)-HL⁵(Cl), inhibited the significant growth of MCF-7 versus T47D cell lines at IC₅₀ concentrations (50% cell inhibition). Additionally, all complexes [Ag(L¹)(Cl)]-[Ag(L⁵)(Cl)] including one of the proligands HL⁴(Cl) showed cytotoxicity results in MCF-7 and T47D with IC₅₀ values below 20 μM. Moreover, HL⁴(Cl), [Ag(L¹)(Cl)], [Ag(L³)(Cl)] and [Ag(L⁵)(Cl)] exhibited cytotoxicity (IC₅₀ values of 16, 13, 16, 15 μM) close to that of Tamoxifen toward MCF-7 cells, Table 5. Interestingly, [Ag(L⁴)(Cl)] (IC₅₀: 9 ± 1.04, 11 ± 1.34) and [Pd(L⁴)(py)(Br)₂], (12) (IC₅₀: 12 ± 1.02, 13 ± 2.83) exhibited cytotoxicity comparable to that of tamoxifen (IC₅₀: 11 ± 1.34, 13 ± 0.71). Considerable, factors such as silver binding, high solubility, and optimized ligand structure may contribute to the observed high cytotoxicity of [Ag(L⁴)(Cl)] against MCF-7 and T47D.

Additionally, the IC₅₀ value of all complexes was greater than 80 μM after 72 h incubation against the Vero cell line (normal cells). However, the silver complexes showed inhibition above 100 μM. The reduced toxicity of the silver complexes toward normal cells may be due to the natural protective ability of silver against cancer (deregulated) cells only and the inability to deregulate normal cell cycle checkpoints, including the inhibition of DNA synthesis and cell division until concentrations exceed 100 μM. Moreover, stronger binding interactions with DNA or tight regulatory inhibition in the cell cycle stages of cancer cells might be identified as important factors contributing to the higher activity of these compounds, along with their solubility in water as pharmacokinetic properties.

A dose-dependent decrease in cell viability was observed in MCF-7 cells (see Figure 12) when treated with [Ag(L⁴)(Cl)] (10) and Tamoxifen. Interestingly, compound 10 at the lowest concentrations of 7.81 and 3.91 μM induced a greater than 30% reduction in cell viability. Moreover, at a concentration of 1.95 μM, the complex demonstrated a > 20% reduction in cell viability, a response not as pronounced when cells were treated with Tamoxifen at the same concentration (*P* < 0.05). This reduction in viability observed in MCF-7 cells treated with

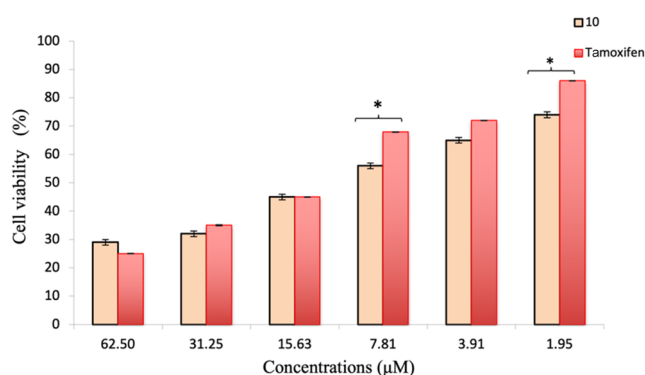


Figure 12. Dose-dependent cell viability in MCF-7 cells against [Ag(L⁴)(Cl)] (10) and Tamoxifen at 48 h. It was done using one-way analysis of variance (ANOVA) in Prism Software Version 9.5.1 and applying the Turkey, Dunnett, and Sedak test to calculate the *P* value (*P* < 0.05).

compound 10 suggests an enhanced sensitivity of MCF-7 toward it.

The cell viability test was done by the adhesion assay for the MCF-7 cell lines with different concentrations of [Ag(L⁴)(Cl)] (10) and Tamoxifen, as depicted in Figure 13. Results of the

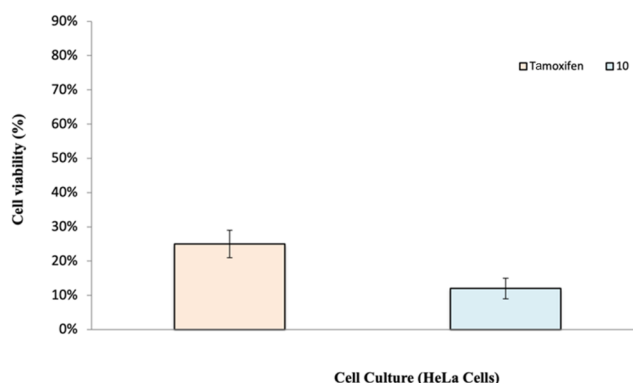


Figure 13. Cell viability by adhesion assay for cell cultures of MCF-7 cell line.

adhesion assay showed that (10) effectively killed MCF-7, whereas Tamoxifen displayed slightly less initial effects on MCF-7 cells. This showed that (10) was able to kill the MCF-7 at a higher rate than Tamoxifen at the initial time of treatment, which might reflect the possible effects of the induction of cell death in MCF-7 after treatment.

2.7. Apoptosis (Phosphatidylserine Exposure) Study.

Apoptosis study (early apoptosis) cells were exposed to IC₅₀ and IC₇₀ doses of [Ag(L⁴)(Cl)] (10) and [Pd(L⁴)(py)(Br)₂] (12) for 12 h. Interestingly, treatments of compounds 10 and 12 caused a green hue in Annexin-FITC staining, indicating phosphoserine (PS) exposure (Figure 14). Both early (green staining) and late (red staining with PI) apoptosis inductions were observed after the 12-h interval. Apoptosis (Annexin V +/PI+) emerged as the predominant mode of cell death, whereas necrosis (Annexin V−/PI+) was infrequent. Apoptosis, or programmed cell death, is a meticulously regulated physiological process well documented in the literature.^{63,64} An early and distinct hallmark of apoptosis is the loss of aminophospholipid (PS) asymmetry in the plasma membrane. It is this disruption of asymmetry that causes phosphatidylser-

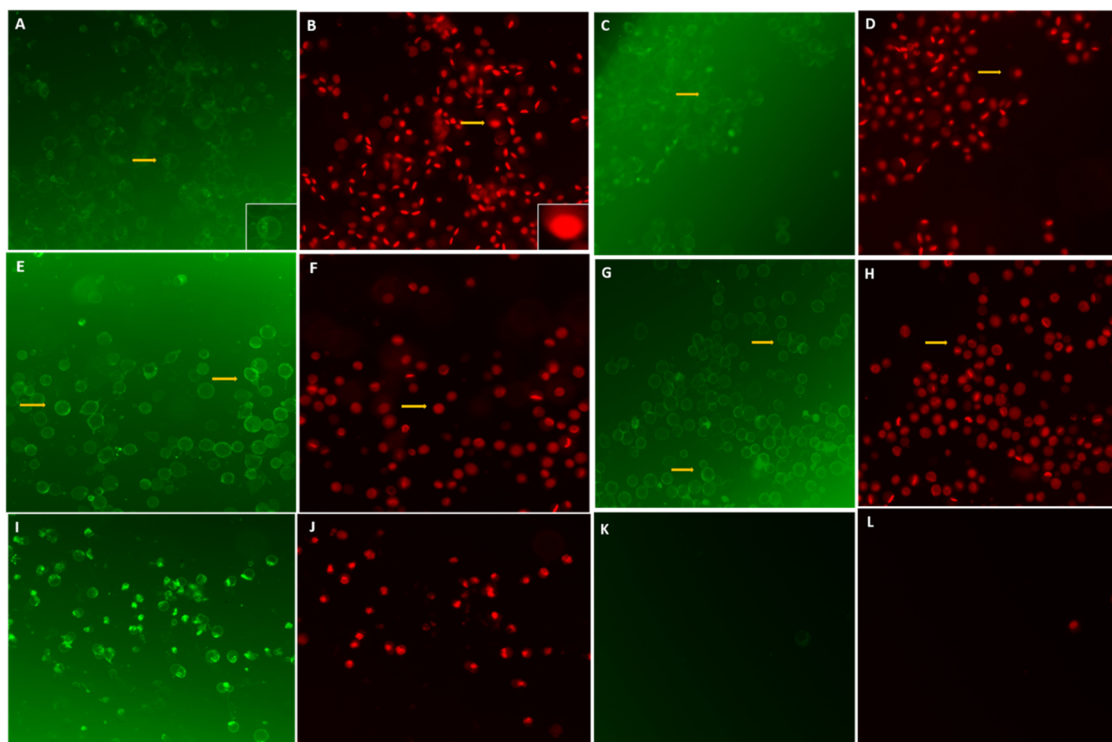


Figure 14. Induction of apoptosis (annexin V and propidium iodide PI) in MCF-7 after treatment with $[\text{Ag}(\text{L}^4)(\text{Cl})]$ (**10**) and $[\text{Pd}(\text{L}^4)(\text{py})(\text{Br})_2]$ (**12**) for 12 h at IC_{50} (A, B and C, D, respectively) and IC_{70} (E, F and G, H, respectively) concentrations. The cells were treated with Tamoxifen (+ve control) and -ve control for 12 h at IC_{50} (I, J and K, L, respectively).

ine (PS) proteins to move to the outer leaflet of the cell membrane in the early stages of apoptosis. Annexin V-FITC, which binds to the exposed PS on the cell membrane surface, enables the detection of the green fluorescence characteristic of apoptosis. Complete or late apoptosis was discerned with the aid of propidium iodide (PI), a red fluorescent dye utilized to stain cellular DNA.^{65–666768697071} On the other hand, staining with annexin V FITC or PI was not evident in untreated negative control cells but was present in positive control cells. PS release from the intracellular milieu to the plasma membrane signals macrophages to engulf apoptotic cells. By inducing apoptosis in cancer cells, this investigation demonstrated that **10** and **12** were capable of eliciting cell demise via apoptosis induction. The degree and pattern of induction remained consistent across both low IC_{50} and high IC_{70} inhibitory concentrations. Notably, IC_{70} inhibitory concentrations also exhibited a positive induction of apoptosis attributable to PS exposure, a phenomenon that is particularly pronounced in cells treated with IC_{50} inhibitory concentrations. This underscores the ability of compounds **10** and **12** to induce cell death predominantly through the apoptosis route (Annexin V+/PI+), as opposed to necrosis (Annexin V-/PI+). Future studies exploring signaling pathways may elucidate the comprehensive mechanism through which apoptosis occurs.

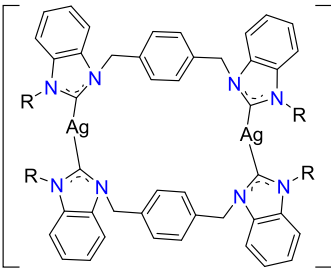
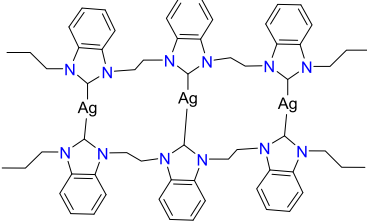
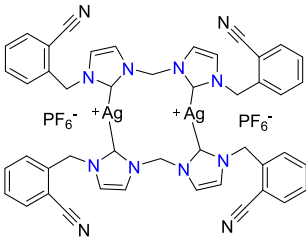
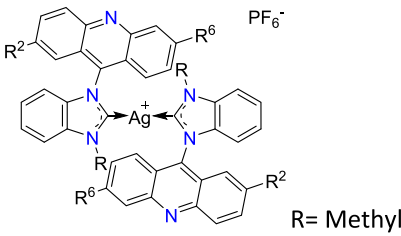
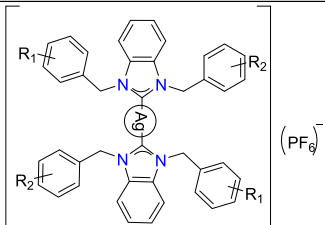
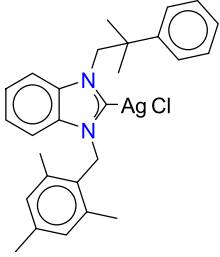
Table 6 compares the findings of reported silver(I) NHC complexes with present work based on their IC_{50} values which specify their cytotoxic effectiveness. MCF-7 cell lines were used for this specific comparison purpose, although limited data are available using a standard drug (Tamoxifen). In Table 6 serial number 3, the silver complex demonstrated significant cytotoxic activity with the lowest IC_{50} value $0.5 \pm 0.1 \mu\text{M}$ as compared to tamoxifen ($2.4 \pm 0.1 \mu\text{M}$). The current study

comprises a mononuclear silver complex, while the other involves di- and trinuclear silver complexes. Despite this fact, the cytotoxic activity of $[\text{Ag}(\text{L}^4)(\text{Cl})]$ was comparable to that of standard drug and better than other complexes except the complex mentioned at serial number 3. This comparison encouraged us to prepare mononuclear silver(I) benzimidazole complexes with the aim of better cytotoxic activity with lower concentrations of silver complexes.

3. EXPERIMENTAL SECTION

3.1. Chemical and Instruments. The synthesis of proligands and complexes was carried out under an inert medium. Silver complexes were synthesized under dark conditions. Consumed chemicals and ingredients were purchased from Sigma-Aldrich and used without further purification unless otherwise stated. Reaction solvents were further dried over NaH and stored in a molecular sieve (3 Å) in an airtight container. Furthermore, analytical grade solvents were used for recrystallization and washing of the compounds. Commercially available grades of silver oxide and aryl halides were used. Melting points of prepared compounds were obtained using open-ended capillaries on a 9200 nm electrothermal melting point apparatus. Elemental analysis was determined by an Element analyzer EAXU0202, Japan. HR ESI-MS was performed on a Shimadzu GC-MS instrument in positive mode. IR spectra were recorded on a PerkinElmer 100 spectrometer ($400\text{--}4000 \text{ cm}^{-1}$). ^1H and ^{13}C NMR was recorded using Bruker Avance 400 HD NMR and JEOL 600 MHz NMR instrument in $d\text{-chloroform}$. TMS was used as an internal standard, while CDCl_3 was used as a reference to record chemical shifts in ppm. Single-crystal XRD technique was used to analyze the single crystal of synthesized compounds. Calf thymus DNA was purchased from Sigma-

Table 6. Comparative Analysis of IC₅₀ Values of Silver NHC Complexes with Reported Literature Values^a

1		43.7 μM	Tamoxifen ⁶⁷ 35.9 μM
2		6.35 ± 0.6 μM	Tamoxifen ⁶⁸ 19.7 ± 0.3 μM
3		0.5 ± 0.1 μM	Tamoxifen ⁶⁹ 2.4 ± 0.1 μM
4		20 ± 3 μM	Tamoxifen ⁷⁰ 11 ± 1
5		20.7 ± 0.4 μM	Tamoxifen ⁷¹ 36 ± 1
Present work		9 ± 1.04 μM	Tamoxifen 11 ± 1.34 μM
MCF-7 cell lines were used in all cases. The standard drug was taken as Tamoxifen			

^aMCF-7 cell lines were used in all cases. The standard drug was taken as Tamoxifen.

Aldrich and the absorbance ratio was measured as 1.8–1.9 (A260/A280) to confirm the purity of CT-DNA before use. This ratio of absorbance showed that DNA was free of protein. The concentration of calf thymus DNA per nucleotide phosphate was determined by absorbance at 258 nm using $6600 \text{ M}^{-1} \text{ cm}^{-1}$. Stock solution of DNA was prepared in Tris-HCl (5 mM) and NaCl (50 mM) mixture (Tris-HCl buffer) while maintaining pH 7.4 and stored at 4 °C. Sample solutions were prepared by dissolving compounds in 0.5% of total volume DMSO and then diluted using Tris-HCl buffer to record the absorption pattern. Precursors **1**, **2**, **HL²(Cl)**, **HL³(Cl)**, **HL⁵(Cl)**, and **[Pd(L⁴)(py)(Br)₂]**, (Pd-PEPPSI) were also reported as direct C–H coupling catalysts.²⁸

3.2. General Procedure for the Synthesis of BNHC Ligands (HL¹(Cl)–HL⁵(Cl)). 1-Cyclopentyl-2,3-dihydro-1H-benzimidazole (**1**) and 1-(2-phenylpropan-2-yl)-2,3-dihydro-1H-benzimidazole (**2**) (1 equiv) were reacted with different aryl halides (1.05 equiv) in dry toluene (25 mL) under argon. Dry Schlenk (50 mL) was pretreated with argon followed by the addition of reagents. The reaction mixture was refluxed for 72 h. Upon precipitation, the mixture was treated with ether to get enough yields. The final product was dried, and yield was calculated (78%).

3.3. HL¹(Cl). ¹H NMR (400 MHz, CDCl₃) δ 11.64 (d, J = 5.7 Hz, 1H, C1), 7.87 (dd, J = 6.4, 3.0 Hz, 1H, C2), 7.79–7.68 (m, 1H, C3), 7.67 (dd, J = 6.3, 3.2 Hz, 2H, C4,5), 5.02–4.95 (p, 1H, C6), 5.93–4.92 (m, 2H, C7), 3.91 (d, J = 4.5 Hz, 2H, C8), 3.29 (d, J = 1.7 Hz, 3H, C9), 2.45 (dd, J = 12.7, 6.1 Hz, 2H, C10), 2.30 (dd, J = 13.5, 6.7 Hz, 2H, C11), 2.09 (dd, J = 7.0 Hz, 2H, C12), 1.98–1.75 (dd, 2H, C13). ¹³C NMR (101 MHz, CDCl₃) δ 142.32 (NCHN), 132.78, 130.83, 126.88, 126.70, 114.48, 113.18, 71.12, 60.02, 59.00, 47.66, 32.22, 23.78. IR (cm⁻¹): 3383, 2982, 2872, 1615, 1560, 1482, 1425, 1353, 1273, 1226, 783, 769, 573. Elemental analysis, calculated for C₁₅H₂₂ClN₂O; C: 63.77, H: 7.59, N: 9.51; found: C: 63.61, H: 7.57, N: 9.48. HR ESI-MS (CH₃CN) m/z calculated for $[M - Cl]^+$ = 245.1653; found: 245.1625.

3.4. HL⁴(Cl). ¹H NMR (400 MHz, CDCl₃) δ 10.18 (s, 1H, C1), 7.32–7.27 (m, 2H, C2, C3), 7.23 (d, J = 7.6 Hz, 2H, C4, C5), 7.16 (t, J = 7.5 Hz, 3H, C6, C7, C10), 7.09 (dd, J = 9.0, 4.1 Hz, 2H, C8, C9), 6.84 (s, 2H, C11, C12), 5.60 (s, 2H, C13), 4.79 (s, 2H, C14), 2.25 (s, 3H, C15), 2.15 (s, 6H, C16, C17), 1.46 (s, 6H, C18, C19). ¹³C NMR (101 MHz, CDCl₃) δ 144.01 (NCHN), 143.95, 139.62, 137.86, 132.47, 130.70, 130.18, 128.89, 127.24, 126.61, 126.21, 124.85, 113.54, 113.11, 59.17, 46.87, 40.07, 26.64, 21.10, 20.21. IR (cm⁻¹): 3123, 3017, 2961, 1614, 1561, 1433, 1335, 1265, 1188, 1151, 762, 752, 5534, 1478. Elemental analysis, calculated for C₂₇H₃₂ClN₂; C: 77.80, H: 7.68, N: 6.59; found: C: 77.45, H: 7.62, N: 6.48. HR ESI-MS (CH₃CN) m/z calculated for $[M - Cl]^+$ = 383.2487; found: 383.2446.

3.5. General Procedure for the Synthesis of Ag-BNHC Complexes ([Ag(L¹)(Cl)]–[Ag(L⁵)(Cl)]). Silver(I) NHCs were prepared following documented procedures with suitable changes.¹⁴ The benzimidazolium salts (300 mg, 74 mmol, 1.00 equiv) were added in a one-armed dry Schlenk flask under argon. After that dry dichloromethane (5 mL) was added under an inert medium and wrapped with aluminum foil to ensure dark condition. Silver(I) oxide (163 mg, 70 mmol, 1.05 equiv) was added into the reaction medium along with a magnetic stirrer and kept stirring at room temperature for 24 h. Upon completion of the reaction, a silver mirror appeared inside the reaction flask. Afterward, the mixture was filtered

over Celite under a vacuum, and the supernatant was separated from the filtrate. Filtration was performed twice to ensure clear filtration and to eliminate metallic silver. The colorless solid was obtained on evaporation of filtrate by rotary evaporator, and recrystallization was done in dichloromethane and ether (2:10) to get fine crystals. The pure product was colorless, and the yield was 88%.

3.6. [Ag(L¹)(Cl)]. ¹H NMR (400 MHz, CDCl₃) δ 7.53 (d, J = 7.2 Hz, 1H, C2), 7.50–7.41 (m, 1H, C3), 7.36–7.22 (m, 2H, C4, C5), 5.31–5.04 (m, 1H, C6), 4.56 (d, J = 4.4 Hz, 2H, C7), 3.76 (t, J = 5.0 Hz, 2H, C8), 3.31–3.11 (m, 3H, C9), 2.21 (s, 4H, C10, C11), 1.99 (d, J = 4.9 Hz, 2H, C12), 1.87–1.62 (m, 2H, C13). ¹³C NMR (101 MHz, CDCl₃) δ 135.23 (NCHN), 132.38, 123.96, 123.59, 112.53, 112.19, 77.36, 77.25, 77.05, 76.73, 72.02, 62.45, 59.12, 49.57, 31.70, 25.07. IR (cm⁻¹): 3091, 2943, 2870, 1672, 1625, 1475, 1384, 1113, 1014, 575, 521. Elemental analysis, calculated for C₂₁H₂₅AgClN₂O; C: 47.37, H: 5.51, N: 7.19; found: C: 47.14, H: 5.48, N: 7.24. HR ESI-MS (CH₃CN) m/z calculated for $[M - Cl]^+$ = 427.0939; found: 427.2686.

3.7. [Ag(L²)(Cl)]. ¹H NMR (400 MHz, CDCl₃) δ 7.59–7.52 (m, 1H, C1), 7.47–7.40 (m, 3H, C2, C3), 7.34 (dd, J = 7.7, 3.7 Hz, 2H, C11, C12), 7.23 (d, J = 8.3 Hz, 2H, C13, C14), 5.59 (s, 2H, CH₂–C10), 5.22 (dd, J = 17.7, 8.9 Hz, 1H, C11), 2.36–2.24 (m, 4H, C12, C13), 2.07 (s, 2H, C14), 1.91–1.75 (m, 2H, C15), 1.27 (s, 9H, C15, C16, C17). ¹³C NMR (101 MHz, CDCl₃) δ 151.55 (NCHN), 134.42, 132.73, 131.85, 127.00, 125.98, 124.13, 123.72, 112.44, 112.42, 77.35, 77.23, 77.03, 76.71, 62.57, 53.23, 34.58, 31.74, 31.23, 25.07. IR (cm⁻¹): 3083, 2956, 2865, 1605, 1513, 1475, 1387, 1342, 1264, 1117, 793, 679, 611, 565, 544. Elemental analysis, calculated for C₂₃H₂₉AgClN₂; C: 57.84, H: 6.23, N: 5.82; found: C: 57.61, H: 6.19, N: 5.78. HR ESI-MS (CH₃CN) m/z calculated for $[M - Cl]^+$ = 521.0554; found: 521.1767.

3.8. [Ag(L³)(Cl)]. ¹H NMR (400 MHz, CDCl₃) δ 7.55 (d, J = 8.0 Hz, 1H, C2), 7.39–7.29 (m, 3H, C3, C4, C5), 6.98 (s, 2H, C6, C7), 5.47 (s, 2H, C6), 5.17 (p, J = 8.9 Hz, 1H, C9), 2.35 (s, 3H, C10), 2.28 (dd, J = 16.4, 7.6 Hz, 2H, C11), 2.24–2.18 (m, 2H, C12), 2.22 (s, 6H, C15, C16), 2.13–1.99 (m, 2H, C13), 1.88–1.73 (m, 2H, C14). ¹³C NMR (101 MHz, CDCl₃) δ 139.58 (NCHN), 137.49, 130.32, 124.00, 123.78, 112.43, 111.95, 77.34, 77.23, 77.03, 76.71, 63.24, 47.90, 31.53, 25.09, 21.20, 20.47. IR (cm⁻¹): 2946, 2865, 1670, 1607, 1474, 1378, 1327, 1193, 1039, 863, 780, 624, 554. Elemental analysis, calculated for C₂₂H₂₇AgClN₂; C: 56.57, H: 5.98, N: 5.79; found: C: 56.17, H: 5.95, N: 5.74. HR ESI-MS (CH₃CN) m/z calculated for $[M - Cl]^+$ = 425.1146; found: 425.1094.

3.9. [Ag(L⁴)(Cl)]. ¹H NMR (400 MHz, CDCl₃) δ 7.32–7.27 (m, 2H, C2, C3), 7.23 (dd, J = 7.7, 3.4 Hz, 3H, C8, C9, C10), 7.17 (d, J = 3.3 Hz, 2H, C4, C5), 7.11 (d, J = 9.2 Hz, 1H, C6), 6.99 (d, J = 6.7 Hz, 1H, C7), 6.94 (s, 2H, C11, C12), 5.41 (s, 2H, C13), 4.49 (s, 2H, C14), 2.33 (s, 3H, C15), 2.16 (s, 6H, C16, C17), 1.51 (s, 6H, C18, C19). ¹³C NMR (101 MHz, CDCl₃) δ 144.04 (NCHN), 138.29, 136.34, 133.93, 133.86, 132.55, 132.48, 129.17, 128.08, 125.90, 125.61, 125.18, 111.40, 110.34, 76.32, 76.21, 76.01, 75.69, 61.02, 47.26, 39.43, 26.51, 20.13, 19.55. IR (cm⁻¹): 2962, 2922, 2869, 1662, 1610, 1477, 1392, 1335, 1261, 743, 669, 643, 566. Elemental analysis, calculated for C₂₇H₃₁AgClN₂; C: 61.55, H: 5.93, N: 5.32; found: C: 61.72, H: 5.92, N: 5.28. HR ESI-MS (CH₃CN) m/z calculated for $[M - Cl]^+$ = 489.1459; found: 489.2300.

3.10. [Ag(L⁵)(Cl)]. ¹H NMR (400 MHz, CDCl₃) δ 7.34 (d, J = 8.0 Hz, 1H, C2), 7.30–7.24 (m, 2H, C3, C4), 7.20 (dd, J =

14.1, 7.0 Hz, 4H, C5, C6, C7, C8), 7.21–7.17 (d, $J = 7.2$ Hz, 1H, C9), 6.97 (m, 1H, C10), 5.39 (s, 2H, C11), 4.46 (s, 2H, C12), 2.33 (s, 3H, C13), 2.27 (s, 6H, C18, C19), 2.13 (s, 6H, C16, C17), 1.48 (s, 6H, C14, C15). ^{13}C NMR (101 MHz, CDCl_3) δ 145.14 (NCHN), 137.10, 134.81, 134.06, 133.80, 132.87, 128.96, 126.75, 126.48, 126.25, 123.74, 123.49, 112.45, 110.99, 48.01, 40.43, 27.54, 17.40, 17.20, 17.14. IR (cm^{-1}); 2955, 1603, 1444, 1390, 1334, 1314, 1181, 1016, 774, 703, 566. Elemental analysis, calculated for $\text{C}_{29}\text{H}_{35}\text{AgClN}_2$; C: 61.77; H: 6.36; N: 5.05; found C: 61.47, H: 6.09, N: 4.93. HR ESI-MS (CH_3CN) m/z calculated for $[\text{M} - \text{Cl}]^+ = 517.1772$; found: 517.1716.

3.11. Cell Culturing. The human cancer cell lines MCF-7 and T47D, along with the primary cell line (Vero), undergo cultivation and maintenance using complete RPMI 1640 medium (Gibco Life Technologies). The Gibco media was supplemented with 10% fetal calf serum (FCS) and 1% antibiotics, specifically 100 IU/mL penicillin and 100 g/mL streptomycin for complete media. The cells are kept in a humidified environment with 5% CO_2 at 37° to ensure optimal growth conditions.

3.12. Cytotoxicity Assay (MTT Assay). We employed the MTT assay (3-(4,5-dimethylthiazol-2-yl)-2,5-diphenyl-2H-tetrazolium bromide) reagent to assess the cytotoxicity of the sample. This assay was conducted in 96-well plates, following the reported procedure. Specifically, 2×10^4 cells were seeded per well, and the plates were then placed in a CO_2 incubator at 37 °C. Various concentrations of compounds in the culture medium (ranging from 1.95 to 500.0 μM) were prepared, and the medium was replenished after 24 h. Following a total incubation period of 48 h, 20 μL of MTT solution was added to each well and allowed to incubate for 3 h. We subsequently measured the optical density at a wavelength of 490 nm using an ELISA reader (Multiscan; ThermoFisher) to evaluate the cytotoxicity.

3.13. Cytotoxicity and Cell Adhesion Assay. We evaluated cell viability using a cell adhesion assay. MCF-7 cells were seeded individually in a 24-well plate at a density of 5×10^5 cells per well and incubated overnight at 37 °C. To assess the impact on cancer cell lines, the cells were treated individually with $[\text{Ag}(\text{L}^4)(\text{Cl})]$ (lowest IC₅₀) and tamoxifen at concentrations ranging from 500 to 1.95 μM for 45 min. We quantified the number of adherent cells (live cell percentage) and nonadherent cells (percentage of dead cells) using a hemocytometer.

3.14. Apoptosis (Phosphatidylserine Exposure) Study. The study focused on determining the induction of apoptosis in the treated cells. The MCF-7 breast cancer cell lines underwent Annexin V/PI staining, following a previously outlined methodology, to discern the modality of cell death or apoptosis induction. Cultivation of cells was performed at a density of 2×10^4 cells per well. Next, we replaced the medium with fresh media that contained $[\text{Ag}(\text{L}^4)(\text{Cl})]$ and $[\text{Pd}(\text{L}^4)(\text{py})(\text{Br})_2]$ treatments at IC₅₀ and IC₇₅ concentrations, which we applied for 12 h at 37 °C. We deliberately chose these two concentrations to elucidate apoptosis induction at both low and high levels. Negative control cells were cultured in a complete medium supplemented with 1% (v/v) DMSO. The apoptosis study was conducted, and images were captured utilizing a Nikon ECLIPSE Ti₂ inverted microscope based in the USA.

3.15. DNA Methodology. Calf thymus DNA (CT-DNA) was purchased from Sigma-Aldrich. A stock solution of CT-

DNA was prepared by dissolving its small amount (0.01 mg) in a buffer system (5 mM Tris-HCl and 50 mM NaCl) of pH 7.4. The solution was stirred overnight in deionized water and kept at 4 °C. The DNA concentration was measured from absorption spectroscopy by considering the molar absorption coefficient ($6600 \text{ M}^{-1} \text{ cm}^{-1}$) at 260 nm. The compound's solutions (0.01 mM) were prepared in a DMSO/buffer system (DMSO was 0.5% of total volume), and the desired concentration was obtained by dilution. The absorbance ratio at A₂₆₀/A₂₈₀ falls in the range of 1.8 to 1.9 to ensure DNA purity. A quartz cell with a path length of 0.1 cm was used to conduct experiments.

3.16. Viscosity Measurements. Viscosity measurements were carried out to check the binding mode of compounds $[\text{Ag}(\text{L}^4)(\text{Cl})]$ and $\text{HL}^4(\text{Cl})$ by keeping CT-DNA concentration constant (0.5 mM) and varying the concentration of compounds by using an Ostwald viscometer at 25 °C. The experiments were conducted three times, and the average flow time was calculated by using a stopwatch. Results were calculated from the equation $\eta = (t - t^\circ)/t^\circ$, where t represents the flow time of the compound, t° indicates the flow time of compound-DNA adduct, and η is the viscosity of the solution. A graph was plotted to show the experimental outcomes with $[\text{compound}/\text{DNA}]$ on the x -axis and $(\eta/\eta^\circ)^{1/3}$ on the y -axis. Here, η shows the viscosity of DNA in the presence of the compound, while η° represents the viscosity in the absence of the compound.

3.17. Molecular Docking Protocols. The structures of the compound were constituted on ACD/ChemSketch 2021.2.1 followed by 3D optimizations and were saved as MDL MOL files. These files were converted to the PDB file format by employing Open Babel GUI⁷² and the protein structures were acquired from RCSB Protein Databank⁷³ followed by their preparation and optimization. AutoDock-Tools-1.5.7⁷⁴ was used for molecular docking studies with the grid box parameters adjusted separately for each protein according to their dimensions and docking was carried out under the preset parameters except the number of GA runs was increased to 200 iterations to obtain greater accuracy where the docked complexes were visualized and analyzed using Discovery Studio 2021 Client.

4. CONCLUSIONS

We investigated a new series of mononuclear benzimidazole-bearing NHC complexes and assessed their cytotoxicity against MCF-7 and T47D and normal cell lines. All complexes demonstrated significant activity, while $[\text{Ag}(\text{L}^4)(\text{Cl})]$ showed superior IC₅₀ values (9 ± 1.04 and 11 ± 1.41) as compared to tamoxifen used as a standard drug (11 ± 1.34 and 13 ± 0.71). The antiproliferative activity of $[\text{Ag}(\text{L}^4)(\text{Cl})]$ is maximized by the synergistic effect of its corresponding proligand ($\text{HL}^4(\text{Cl})$). Notably, $\text{HL}^4(\text{Cl})$ also showed enhanced activity, evidenced in terms of IC₅₀ (16 ± 0.77) seemingly close to that of silver NHC complexes. Anticancer assay underscores the ability of compounds to induce cell death predominantly through the apoptosis route (Annexin V+/PI+), as opposed to necrosis (Annexin V−/PI+). Additionally, for $[\text{Pd}(\text{L}^4)(\text{py})(\text{Br})_2]$, the complex was also tested against the cancerous cell lines to further explore the synergistic effect exhibited by BNHC ligands on metal centers. $[\text{Ag}(\text{L}^4)(\text{Cl})]$ was employed in DNA binding studies to explore the binding mode of complexes with CT-DNA. Stability studies were conducted in phosphate-buffered saline, and Tris-HCl (pH 7.4) results showed no

significant spectral changes over a period of 72 h under physiological conditions, indicating the withstanding of complexes in an alkaline buffer system. In molecular docking, binding patterns and binding energies of the screened candidates were found to be in good agreement with the experimentally determined anticancer potency.

■ ASSOCIATED CONTENT

SI Supporting Information

The Supporting Information is available free of charge at <https://pubs.acs.org/doi/10.1021/acsomega.4c11048>.

Crystallographic data (CIF)

Crystallographic data (CIF)

Crystallographic data (CIF)

Detailed characterization data, additional figures, and tables (PDF)

■ AUTHOR INFORMATION

Corresponding Authors

Gul-e-Saba Chaudhry – Institute of Climate Adaptation and Marine Biotechnology, Universiti Malaysia Terengganu, 21030 Kuala Terengganu, Malaysia; Email: gul.saba@umt.edu.my

Ismail Özdemir – Catalysis Research and Application Centre, Inönü University, 44210 Malatya, Türkiye; Faculty of Science and Art, Department of Chemistry, İnönü University, 44210 Malatya, Türkiye; Email: ismail.ozdemir@inonu.edu.tr

Muhammad Naveed Zafar – Department of Chemistry, Quaid-I-Azam University, 45320 Islamabad, Pakistan; orcid.org/0000-0003-1061-4332; Email: mnzafar@qau.edu.pk

Authors

Naima Munir – Department of Chemistry, Quaid-I-Azam University, 45320 Islamabad, Pakistan; Catalysis Research and Application Centre, Inönü University, 44210 Malatya, Türkiye

Navin Gürbüz – Catalysis Research and Application Centre, Inönü University, 44210 Malatya, Türkiye; Faculty of Science and Art, Department of Chemistry, İnönü University, 44210 Malatya, Türkiye

Muhammad Sarfraz – Institute of chemistry, Islamia University of Bahawalpur, 63100 Bahawalpur, Pakistan

Betül Şen – Department of Physics, Faculty of Arts and Sciences, Dokuz Eylül University, 35150 İzmir, Türkiye

Muhittin Aygün – Department of Physics, Faculty of Arts and Sciences, Dokuz Eylül University, 35150 İzmir, Türkiye

Complete contact information is available at:

<https://pubs.acs.org/doi/10.1021/acsomega.4c11048>

Notes

The authors declare no competing financial interest.

■ ACKNOWLEDGMENTS

The authors express their deep gratitude to the Türkiye Burslari Scholarship at Inonu University Malatya Turkey (Scholarship ID: 21PK070710) and HEC for IRSIP Scholarship to Kyushu University, Japan.

■ REFERENCES

- (1) Sung, H.; Ferlay, J.; Siegel, R. L.; Laversanne, M.; Soerjomataram, I.; Jemal, A.; Bray, F. Global cancer statistics 2020: GLOBOCAN estimates of incidence and mortality worldwide for 36 cancers in 185 countries. *Ca-Cancer J. Clin.* **2021**, *71* (3), 209–249.
- (2) Kocarnik, J. M.; Compton, K.; Dean, F. E.; Fu, W.; Gaw, B. L.; Harvey, J. D.; Henrikson, H. J.; Lu, D.; Pennini, A.; Xu, R. Cancer incidence, mortality, years of life lost, years lived with disability, and disability-adjusted life years for 29 cancer groups from 2010 to 2019: a systematic analysis for the global burden of disease study 2019. *JAMA Oncol.* **2022**, *8* (3), 420–444.
- (3) Sui, X.; Niu, X.; Zhou, X.; Gao, Y. Peptide drugs: a new direction in cancer immunotherapy. *Cancer Biol. Med.* **2024**, *21* (3), 198–203.
- (4) Santucci, C.; Mignozzi, S.; Malvezzi, M.; Boffetta, P.; Collatuzzo, G.; Levi, F.; La Vecchia, C.; Negri, E. European cancer mortality predictions for the year 2024 with focus on colorectal cancer. *Ann. Oncol.* **2024**, *35* (3), 308–316.
- (5) Rajesh, A.; Easley, E.; Madu, C. O.; Lu, Y. *The Role of Estrogen Receptors and Signaling Pathways in Breast Cancer*; IntechOpen, 2024.
- (6) Ghosh, S. Cisplatin: The first metal based anticancer drug. *Bioorg. Chem.* **2019**, *88*, No. 102925.
- (7) Zengin Kurt, B.; Öztürk Civelek, D.; Cakmak, E. B.; Kolcuoğlu, Y.; Şenol, H.; Sağlık Özkan, B. m. N.; Dag, A.; Benkli, K. Synthesis of Sorafenib– Ruthenium Complexes, Investigation of Biological Activities and Applications in Drug Delivery Systems as an Anticancer Agent. *J. Med. Chem.* **2024**, *67* (6), 4463–4482.
- (8) Deng, L.; Sathyan, A.; Adam, C.; Unciti-Broceta, A.; Sebastian, V.; Palmans, A. R. Enhanced Efficiency of Pd (0)-Based Single Chain Polymeric Nanoparticles for in Vitro Prodrug Activation by Modulating the Polymer's Microstructure. *Nano Lett.* **2024**, *24*, 2242–2249.
- (9) Liang, H.; Huang, W.; Xu, X.; Zou, D.; Wang, Y.; Yin, F. Rhodium (I) Complexes Containing the N \wedge N \wedge N-Chelating Ligand: Synthesis, Structure, and Biological Activity. *Organometallics* **2024**, *43* (2), 108–118.
- (10) He, G.; Pan, Y.; Zeng, F.; Qin, S.; Luan, X.; Lu, Q.; Xie, C.; Hu, P.; Gao, Y.; Yang, J.; et al. Microfluidic Synthesis of CuH Nanoparticles for Antitumor Therapy through Hydrogen-Enhanced Apoptosis and Cuproptosis. *ACS Nano* **2024**, *18* (12), 9031–9042.
- (11) Shahraki, S.; Delarami, H. S.; Razmara, Z.; Heidari, A. Tracking the binding site of anticancer drug fluxoridin with Fe-related proteins to achieve intelligent drug delivery. *Spectrochim. Acta, Part A* **2024**, *306*, No. 123569.
- (12) Zhang, C.; Zhang, N.; Niu, W.; Li, R.; Liu, Y.; Mu, Y.; Xu, C.; Yao, Q.; Gao, X. Ultrasmall platinum nanoclusters: A potent chemotherapeutic drug for cancer-specific DNA damage with optimizing therapeutic efficacy while minimizing systemic toxicity. *Nano Today* **2024**, *55*, No. 102195.
- (13) Mariconda, A.; Iacopetta, D.; Sirignano, M.; Ceramella, J.; Costabile, C.; Pellegrino, M.; Rosano, C.; Catalano, A.; Saturnino, C.; El-Kashef, H.; et al. N-Heterocyclic Carbene (NHC) Silver Complexes as Versatile Chemotherapeutic Agents Targeting Human Topoisomerases and Actin. *ChemMedChem* **2022**, *17* (18), No. e202200345.
- (14) Wong, C. H.; Khor, B.-K.; Inggang, G. T. J. K. A.; Affandi, N. A. M. N.; Murugaiyah, V.; Chear, N. J.-Y.; Yam, W. Effect of fluorination on the cytotoxic potentials of benzimidazolium-based N-heterocyclic carbene ligands and their silver (I) complexes. *Inorg. Chim. Acta* **2024**, *567*, No. 122040.
- (15) Varna, D.; Geromichalos, G.; Gioftsos, D. K.; Tzimopoulos, D.; Hatzidimitriou, A. G.; Dalezis, P.; Papi, R.; Trafalis, D.; Angaridis, P. A. N-heterocyclic-carbene vs diphosphine auxiliary ligands in thioamidato Cu (I) and Ag (I) complexes towards the development of potent and dual-activity antibacterial and apoptosis-inducing anticancer agents. *J. Inorg. Biochem.* **2024**, *252*, No. 112472.
- (16) Lin, K.; Jia, X.; Zhang, X.; Li, W.; Wang, B.; Wang, Z.; Xue, X.; Fan, X.; Ma, Z. Synthesis, characterization, antiproliferative activity and DNA binding calculation of substituted-phenyl-terpyridine copper (II) nitrate complexes. *J. Inorg. Biochem.* **2023**, *250*, No. 112418.
- (17) Akbari, Z.; Stagno, C.; Iraci, N.; Efferth, T.; Omer, E. A.; Piperno, A.; Montazerzohori, M.; Feizi-Dehmayebi, M.; Micale, N.

Biological evaluation, DFT, MEP, HOMO-LUMO analysis and ensemble docking studies of Zn (II) complexes of bidentate and tetradentate Schiff base ligands as antileukemia agents. *J. Mol. Struct.* **2024**, *1301*, No. 137400.

(18) Tonon, G.; Mauceri, M.; Cavarzerani, E.; Piccolo, R.; Santo, C.; Demitri, N.; Orian, L.; Nogara, P. A.; Rocha, J. B. T.; Canzonieri, V.; et al. Unveiling the promising anticancer activity of palladium (II)-aryl complexes bearing diphosphine ligands: a structure-activity relationship analysis. *Dalton Trans.* **2024**, *53*, 8463–8477.

(19) Franco Machado, J.; Cordeiro, S.; Duarte, J. N.; Costa, P. J.; Mendes, P. J.; Garcia, M. H.; Baptista, P. V.; Fernandes, A. R.; Morais, T. S. Exploiting Co (III)-Cyclopentadienyl Complexes To Develop Anticancer Agents. *Inorg. Chem.* **2024**, *63*, 5783–5804.

(20) Nolan, S. P.; Ma, X.; Caligiuri, I.; Rizzolio, F.; Bracho, N.; Van Hecke, K.; Scattolin, T. Dinuclear NHC-gold (I)-thiolato and-alkynyl complexes: synthesis, anticancer activity, and catalytic activity in lactonization reactions. *Dalton Trans.* **2024**, *53*, 7939–7945.

(21) Mageed, A. H.; Hadi, I. S. Synthesis and Anticancer Activities of some Ag (I) Complexes Involving N-Heterocyclic Carbene Ligands. *ChemistrySelect* **2024**, *9* (5), No. e202304737.

(22) Bekci, H.; Özdemir, N.; Şahin, Z.; Mumcu, A.; Dayan, S.; Karataş, M. O. New silver, rhodium and iridium complexes with anthracene-functionalized N-heterocyclic carbene ligands: Crystal structures, cytotoxicity and fluorescence studies. *Polyhedron* **2024**, *257*, No. 117011.

(23) Ali, T. H.; Salman, A. W.; Abdulhussein, R. S.; Persoons, L.; Daelemans, D.; Dehaen, W.; Van Meervelt, L. New sugar-incorporated N-heterocyclic carbene precursors and their Ag (I) and Pd (II) complexes: Synthesis, characterization, and cytotoxicity studies. *J. Mol. Liq.* **2024**, *393*, No. 123618.

(24) Zhao, Q.; Han, B.; Peng, C.; Zhang, N.; Huang, W.; He, G.; Li, J. L. A promising future of metal-N-heterocyclic carbene complexes in medicinal chemistry: The emerging bioorganometallic antitumor agents. *Med. Res. Rev.* **2024**, *44*, 2194–2235.

(25) Johnson, N. A.; Southerland, M. R.; Youngs, W. J. Recent developments in the medicinal applications of silver-NHC complexes and imidazolium salts. *Molecules* **2017**, *22* (8), 1263.

(26) Movahedi, E.; Rezvani, A. R. New silver (I) complex with diazafluorene based ligand: synthesis, characterization, investigation of in vitro DNA binding and antimicrobial studies. *J. Mol. Struct.* **2017**, *1139*, 407–417.

(27) Wu, H.; Yuan, J.; Bai, Y.; Pan, G.; Wang, H.; Kong, J.; Fan, X.; Liu, H. Synthesis, structure, DNA-binding properties and antioxidant activity of silver (I) complexes containing V-shaped bis-benzimidazole ligands. *Dalton Trans.* **2012**, *41* (29), 8829–8838.

(28) Munir, N.; Gürbüz, N.; Zafar, M. N.; Evren, E.; Şen, B.; Aygün, M.; Özdemir, İ. Plausible PEPPSI catalysts for direct CH functionalization of furans and pyrroles. *J. Mol. Struct.* **2024**, *1295*, No. 136679.

(29) Ronconi, L.; Sadler, P. J. Using coordination chemistry to design new medicines. *Coord. Chem. Rev.* **2007**, *251* (13–14), 1633–1648.

(30) Yamashita, M.; Hartwig, J. F. Synthesis, structure, and reductive elimination chemistry of three-coordinate arylpalladium amido complexes. *J. Am. Chem. Soc.* **2004**, *126* (17), 5344–5345.

(31) Elsayed, S. A.; El-Gharabawy, H. M.; Butler, I. S.; Atlam, F. M. Novel metal complexes of 3-acetylcoumarin-2-hydrazinobenzothiazole Schiff base: Design, structural characterizations, DNA binding, DFT calculations, molecular docking and biological studies. *Appl. Organomet. Chem.* **2020**, *34* (6), No. e5643.

(32) Arjmand, F.; Jamsheera, A. DNA binding studies of new valine derived chiral complexes of tin (IV) and zirconium (IV). *Spectrochim. Acta, Part A* **2011**, *78* (1), 45–51.

(33) Milutinović, M. M.; Rilak, A.; Bratsos, I.; Klisurić, O.; Vraneš, M.; Gligorijević, N.; Radulović, S.; Bugarčić, Ž. D. New 4'-(4-chlorophenyl)-2, 2': 6', 2''-terpyridine ruthenium (II) complexes: synthesis, characterization, interaction with DNA/BSA and cytotoxicity studies. *J. Inorg. Biochem.* **2017**, *169*, 1–12.

(34) Pratviel, G.; Bernadou, J.; Meunier, B. DNA and RNA cleavage by metal complexes. In *Advances in Inorganic Chemistry*; Elsevier, 1998; Vol. 45, pp 251–312.

(35) Haq, I.; Lincoln, P.; Suh, D.; Norden, B.; Chowdhry, B. Z.; Chaires, J. B. Interaction of delta-and. lambda-[Ru (phen) 2DPPZ] 2+ with DNA: a calorimetric and equilibrium binding study. *J. Am. Chem. Soc.* **1995**, *117* (17), 4788–4796.

(36) Eshkourfu, R.; Cobeljić, B.; Vujčić, M.; Turel, I.; Pevec, A.; Sepčić, K.; Zec, M.; Radulović, S.; Srdić-Radić, T.; Mitić, D.; et al. Synthesis, characterization, cytotoxic activity and DNA binding properties of the novel dinuclear cobalt (III) complex with the condensation product of 2-acetylpyridine and malonic acid dihydrazide. *J. Inorg. Biochem.* **2011**, *105* (9), 1196–1203.

(37) Tarai, S. K.; Tarai, A.; Mandal, S.; Nath, B.; Som, I.; Bhaduri, R.; Bagchi, A.; Sarkar, S.; Biswas, A.; Moi, S. C. Cytotoxic behavior and DNA/BSA binding activity of thiosemicarbazone based Ni (II) complex: bio-physical, molecular docking and DFT study. *J. Mol. Liq.* **2023**, *383*, No. 121921.

(38) Gholivand, M. B.; Peyman, H.; Gholivand, K.; Roshanfekr, H.; Taherpour, A.; Yaghobi, R. Theoretical and instrumental studies of the competitive interaction between aromatic α -aminobisphosphonates with DNA using binding probes. *Appl. Biochem. Biotechnol.* **2017**, *182*, 925–943.

(39) Arshad, N.; Bhatti, M. H.; Farooqi, S. I.; Saleem, S.; Mirza, B. Synthesis, photochemical and electrochemical studies on triphenyltin (IV) derivative of (Z)-4-(4-cyanophenylamino)-4-oxobut-2-enoic acid for its binding with DNA: biological interpretation. *Arabian J. Chem.* **2016**, *9* (3), 451–462.

(40) Carter, M. T.; Bard, A. J. Voltammetric studies of the interaction of tris (1, 10-phenanthroline) cobalt (III) with DNA. *J. Am. Chem. Soc.* **1987**, *109* (24), 7528–7530.

(41) Shujha, S.; Shah, A.; Muhammad, N.; Ali, S.; Qureshi, R.; Khalid, N.; Meetsma, A. Diorganotin (IV) derivatives of ONO tridentate Schiff base: synthesis, crystal structure, in vitro antimicrobial, anti-leishmanial and DNA binding studies. *Eur. J. Med. Chem.* **2010**, *45* (7), 2902–2911.

(42) Thornton, L.; Dixit, V.; Assad, L. O.; Ribeiro, T. P.; Queiroz, D. D.; Kellett, A.; Casey, A.; Colleran, J.; Pereira, M. D.; Rochford, G.; et al. Water-soluble and photo-stable silver (I) dicarboxylate complexes containing 1, 10-phenanthroline ligands: Antimicrobial and anticancer chemotherapeutic potential, DNA interactions and antioxidant activity. *J. Inorg. Biochem.* **2016**, *159*, 120–132.

(43) Swavey, S.; DeBeer, M.; Li, K. Photoinduced interactions of supramolecular ruthenium (II) complexes with plasmid DNA: Synthesis and spectroscopic, electrochemical, and DNA photocleavage studies. *Inorg. Chem.* **2015**, *54* (7), 3139–3147.

(44) Mahadevan, S.; Palaniandavar, M. Spectroscopic and voltammetric studies on copper complexes of 2, 9-dimethyl-1, 10-phenanthrolines bound to calf thymus DNA. *Inorg. Chem.* **1998**, *37* (4), 693–700.

(45) Niranjana, E.; Naik, R. R.; Swamy, B. K.; Bodke, Y. D.; Sherigara, B.; Jayadevappa, H.; Badami, B. Cyclic voltammetric investigations of 3-aryl-4-bromo sydnone and its derivatives at glassy carbon electrode. *Int. J. Electrochem. Sci.* **2008**, *3* (9), 980–992.

(46) García, T.; Revenga-Parra, M.; Abruña, H.; Pariente, F.; Lorenzo, E. Single-mismatch position-sensitive detection of DNA based on a bifunctional ruthenium complex. *Anal. Chem.* **2008**, *80* (1), 77–84.

(47) Phadte, A. A.; Banerjee, S.; Mate, N. A.; Banerjee, A. Spectroscopic and viscometric determination of DNA-binding modes of some bioactive dibenzodioxins and phenazines. *Biochem. Biophys. Rep.* **2019**, *18*, No. 100629.

(48) Satyanarayana, S.; Dabrowiak, J. C.; Chaires, J. B. Neither. DELTA-nor. LAMBDA-tris (phenanthroline) ruthenium (II) binds to DNA by classical intercalation. *Biochemistry* **1992**, *31* (39), 9319–9324.

(49) Cohen, G.; Eisenberg, H. Viscosity and sedimentation study of sonicated DNA–proflavine complexes. *Biopolymers* **1969**, *8* (1), 45–55.

- (50) Ceccherini, V.; Giorgi, E.; Mannelli, M.; Cirri, D.; Gamberi, T.; Gabbiani, C.; Pratesi, A. Synthesis, Chemical Characterization, and Biological Evaluation of Hydrophilic Gold (I) and Silver (I) N-Heterocyclic Carbenes as Potential Anticancer Agents. *Inorg. Chem.* **2024**, 63 (37), 16949–16963.
- (51) Esarev, I. V.; Karge, B.; Zeng, H.; Lippmann, P.; Jones, P. G.; Schrey, H.; Brönstrup, M.; Ott, I. Silver Organometallics that are Highly Potent Thioredoxin and Glutathione Reductase Inhibitors: Exploring the Correlations of Solution Chemistry with the Strong Antibacterial Effects. *ACS Infect. Dis.* **2024**, 10 (5), 1753–1766.
- (52) Frisch, M. J.; Trucks, G. W.; Schlegel, H. B.; Scuseria, G. E.; Robb, M. A.; Cheeseman, J. R.; Scalmani, G.; Barone, V.; Mennucci, B.; Petersson, G. A.; et al. *Gaussian 09*, revision D. 01; Gaussian, Inc.: Wallingford, CT, 2009.
- (53) Stephens, P. J.; Devlin, F. J.; Chabalowski, C. F.; Frisch, M. J. Ab initio calculation of vibrational absorption and circular dichroism spectra using density functional force fields. *J. Phys. Chem. A* **1994**, 98 (45), 11623–11627.
- (54) Vosko, S. H.; Wilk, L.; Nusair, M. Accurate spin-dependent electron liquid correlation energies for local spin density calculations: a critical analysis. *Can. J. Phys.* **1980**, 58 (8), 1200–1211.
- (55) Ben Gzaïel, M.; Oueslati, A.; Chaabane, I.; Gargouri, M. Density functional theory calculations of the molecular structure and the vibrational spectra of bis-tetrapropyl-ammonium hexachloro-dizincate. *J. Mol. Struct.* **2016**, 1122, 280–289.
- (56) Panicker, R. R.; Sivaramakrishna, A. Studies on synthesis and influence of sterically driven Ni (II)-terpyridine (NNN) complexes on BSA/DNA binding and anticancer activity. *J. Inorg. Biochem.* **2024**, 257, No. 112553.
- (57) Morad, R.; Akbari, M.; Maaza, M. Theoretical study of chemical reactivity descriptors of some repurposed drugs for COVID-19. *MRS Adv.* **2023**, 8 (11), 656–660.
- (58) Akl, M. A.; Al-Awadhi, M. M.; El-Zeny, A. S. Divalent transition metal complexes of nitrogen, oxygen and sulfur containing ligand: design, structural, spectral, pH-metric, theoretical molecular modeling, analytical and mechanism studies. *Appl. Water Sci.* **2023**, 13 (10), 195.
- (59) Dolatyari, V.; Shahsavari, H. R.; Fereidoonzehad, M.; Farhadi, F.; Akhlaghi, S.; Latouche, C.; Sakamaki, Y.; Beyzavi, H. Luminescent heterobimetallic PtII–AuI complexes bearing N-Heterocyclic carbenes (NHCs) as potent Anticancer agents. *Inorg. Chem.* **2023**, 62 (33), 13241–13252.
- (60) Ayyaz, M.; Sarfraz, M.; Arshad, M.; Yaqoob, A.; Siddique, S. A.; Hussain, S.; Ali, M. A.; Qureshi, A. M.; Rauf, A. Design, synthesis, in-vitro biological screening and in-silico studies of 2-thioxodihydropyrimidinone based new aminomethylene scaffolds. *J. Mol. Struct.* **2024**, 1299, No. 137153.
- (61) Ilayaraja, R.; Rajkumar, R.; Rajesh, D.; Muralidharan, A. R.; Padmanabhan, P.; Archunan, G. Evaluating the binding efficiency of pheromone binding protein with its natural ligand using molecular docking and fluorescence analysis. *Sci. Rep.* **2014**, 4 (1), No. 5201.
- (62) Siddique, S.; Hussain, K.; Shehzadi, N.; Arshad, M.; Arshad, M. N.; Iftikhar, S.; Saghir, F.; Shaukat, A.; Sarfraz, M.; Ahmed, N. Design, synthesis, biological evaluation and molecular docking studies of quinoline-anthranilic acid hybrids as potent anti-inflammatory drugs. *Org. Biomol. Chem.* **2024**, 22 (18), 3708–3724.
- (63) Jan, R.; Chaudhry, G. e. S. Understanding apoptosis and apoptotic pathways targeted cancer therapeutics. *Adv. Pharm. Bull.* **2019**, 9 (2), 205.
- (64) Fadok, V. A.; Voelker, D. R.; Campbell, P. A.; Cohen, J. J.; Bratton, D. L.; Henson, P. M. Exposure of phosphatidylserine on the surface of apoptotic lymphocytes triggers specific recognition and removal by macrophages. *J. Immunol.* **1992**, 148 (7), 2207–2216.
- (65) Schlegel, R. A.; Williamson, P. Phosphatidylserine, a death knell. *Cell Death Differ.* **2001**, 8 (6), 551–563.
- (66) Gul, I.; Yunus, U.; Ajmal, M.; Bhatti, M. H.; Chaudhry, G. e. S. Development of biodegradable thin films for efficient, specific and controlled delivery of capecitabine. *Biomed. Mater.* **2021**, 16 (5), No. 055019.
- (67) Haque, R. A.; Hasanudin, N.; Iqbal, M. A.; Ahmad, A.; Hashim, S.; Abdul Majid, A.; Ahamed, M. B. K. Synthesis, crystal structures, in vitro anticancer, and in vivo acute oral toxicity studies of bis-imidazolium/benzimidazolium salts and respective dinuclear Ag (I)-N-heterocyclic carbene complexes. *J. Coord. Chem.* **2013**, 66 (18), 3211–3228.
- (68) Abdurrahman, N.; Braim, F. S.; Razali, M. R. Synthesis, Characterization, and Anticancer Studies of Dimethylene Bridged Bis Tri-n-heterocyclic Carbene Trinuclear Silver (I). *Malays. J. Med. Health Sci.* **2024**, 20, 66–74.
- (69) Haque, R. A.; Hasanudin, N.; Hussein, M. A.; Ahamed, S. A.; Iqbal, M. A. Bis-N-heterocyclic carbene silver (I) and palladium (II) complexes: efficient antiproliferative agents against breast cancer cells. *Inorg. Nano-Met. Chem.* **2017**, 47 (1), 131–137.
- (70) Sharhan, O.; Heidelberg, T.; Hashim, N. M.; Al-Madhagi, W. M.; Ali, H. M. Benzimidazolium-acridine-based silver N-heterocyclic carbene complexes as potential anti-bacterial and anti-cancer drug. *Inorg. Chim. Acta* **2020**, 504, No. 119462.
- (71) King, O. S.; Hofmann, B. J.; Boakye-Smith, A. E.; Managh, A. J.; Stringer, T.; Lord, R. M. Fluorinated N-Heterocyclic Carbene Silver (I) Complexes with High Cancer Cell Selectivity. *Organometallics* **2024**, 43 (20), 2662–2673.
- (72) O'Boyle, N. M.; Banck, M.; James, C. A.; Morley, C.; Vandermeersch, T.; Hutchison, G. R. Open Babel: An open chemical toolbox. *J. Cheminf.* **2011**, 3, 1–14.
- (73) Berman, H. M.; Westbrook, J.; Feng, Z.; Gilliland, G.; Bhat, T. N.; Weissig, H.; Shindyalov, I. N.; Bourne, P. E. The protein data bank. *Nucleic Acids Res.* **2000**, 28 (1), 235–242.
- (74) Sanner, M. F. Python: a programming language for software integration and development. *J. Mol. Graphics Modell.* **1999**, 17 (1), 57–61.